

# A blind HI survey in the Ursa Major region <sup>★</sup>

K. Wolfinger<sup>1,2†</sup>, V. A. Kilborn<sup>1</sup>, B. S. Koribalski<sup>2</sup>, R. F. Minchin<sup>3</sup>, P. J. Boyce<sup>4</sup>,  
M. J. Disney<sup>5</sup>, R. H. Lang<sup>5</sup>, C. A. Jordan<sup>6</sup>

<sup>1</sup> Centre for Astrophysics & Supercomputing, Swinburne University of Technology, Mail H39, PO Box 218, Hawthorn, VIC 3122, Australia

<sup>2</sup> CSIRO Astronomy and Space Science, PO Box 76, Epping, NSW 1710, Australia

<sup>3</sup> Arecibo Observatory, HC03 Box 53995, Arecibo, Puerto Rico 00612

<sup>4</sup> Registry, Cardiff University, Cardiff, CF10 3UA, United Kingdom

<sup>5</sup> School of Physics and Astronomy, Cardiff University, Cardiff, CF24 3YB, United Kingdom

<sup>6</sup> Jodrell Bank Observatory, Macclesfield, Cheshire, SK11 9DL, United Kingdom

Accepted 2012 October 4. Received 2012 September 30; in original form 2012 January 31

## ABSTRACT

We have conducted the first blind H I survey covering 480 deg<sup>2</sup> and a heliocentric velocity range from 300–1900 km s<sup>-1</sup> to investigate the H I content of the nearby spiral-rich Ursa Major region and to look for previously uncatalogued gas-rich objects. Here we present the catalog of H I sources. The H I data were obtained with the 4-beam receiver mounted on the 76.2-m Lovell telescope (FWHM 12 arcmin) at the Jodrell Bank Observatory (UK) as part of the H I Jodrell All Sky Survey (HIJASS). We use the automated source finder DUCHAMP and identify 166 H I sources in the data cubes with H I masses in the range of 10<sup>7</sup>–10<sup>10.5</sup> M<sub>⊙</sub>. Our Ursa Major H I catalogue includes 10 first time detections in the 21-cm emission line.

We identify optical counterparts for 165 H I sources (99 per cent). For 54 H I sources (~ 33 per cent) we find numerous optical counterparts in the HIJASS beam, indicating a high density of galaxies and likely tidal interactions. Four of these H I systems are discussed in detail.

We find only one H I source (1 per cent) without a visible optical counterpart out of the 166 H I detections. Green Bank Telescope (FWHM 9 arcmin) follow-up observations confirmed this H I source and its H I properties. The nature of this detection is discussed and compared to similar sources in other H I surveys.

**Key words:** surveys – catalogs – radio emission lines – galaxies: fundamental parameters

## 1 INTRODUCTION

The distribution of galaxies in the Universe is not uniform – galaxies are found in filamentary structures, groups and clusters (e.g. Colless et al. 2001). The observed ‘cosmic web’ structure is in good agreement with numerical simulations according to Cold Dark Matter cosmology (e.g. Springel et al. 2005; Simon & Geha 2007), whereby gravity drives the formation of structure from small, primordial, Gaussian fluctuations. Dark matter haloes grow through merging and accretion of smaller ones. Within the dark matter haloes, galaxies form by cooling of baryons (e.g. White & Rees 1978). Hence, small dark matter haloes are the primordial building blocks of larger structures in the hierarchical model of structure formation.

Dwarf irregular galaxies with low stellar luminosity and low surface brightness galaxies are typically discovered in neutral hydrogen (H I) surveys (Schombert et al. 1992, Minchin et al. 2003, Giovanelli et al. 2005), as they are rich in neutral gas but difficult to detect in optical or infrared surveys. Whilst optical surveys are most sensitive to high surface brightness early-type galaxies (Disney 1976), H I surveys are unbiased by stellar populations and are most likely to detect gas-rich late-type spirals and irregular galaxies. Hence optical and H I surveys complement each other as there is a rough correlation between increasing H I content from early to late type galaxies and decreasing optical surface brightness with morphological type (Toribio et al. 2011). Discoveries in H I surveys also include intriguing objects, e.g. the detection of an H I-massive cloud without stellar counterpart, within the NGC2442 group (Ryder et al. 2001), extended H I arms or tidal tails (Koribalski & López-Sánchez 2009) and H I between galaxies in groups (Koribalski & Manthey 2005, Kilborn et al. 2006, English et al. 2010). Large-area blind H I surveys have been con-

<sup>★</sup> The data cubes were obtained with the Lovell telescope at the Jodrell Bank observatory, UK.

<sup>†</sup> E-mail: kwolfinger@astro.swin.edu.au

ducted such as the Arecibo HI Strip Survey (AHISS, Zwaan et al. 1997), the Arecibo Dual Beam Survey (ADBS, Rosenberg & Schneider 2000), the H I Jodrell All-Sky Survey (HIJASS, Lang et al. 2003), the H I Parkes All-Sky Survey (HIPASS, Staveley-Smith et al. 1996, Barnes et al. 2001, Koribalski et al. 2004, Meyer et al. 2004), the Arecibo Legacy Fast ALFA survey (ALFALFA, Giovanelli et al. 2005) and the Arecibo Galaxy Environment Survey (AGES, Auld et al. 2006). Upcoming H I surveys such as the ASKAP H I All-Sky Survey (known as WALLABY, Koribalski & Staveley-Smith 2009<sup>1</sup>) will further contribute to our knowledge of gas-rich galaxies in the local Universe.

Isolated galaxies tend to have noticeably different properties from galaxies residing in dense regions. Observations have shown that early-type galaxies are common in clusters whereas late-type galaxies dominate the less dense environments (morphology-density relation; e.g. Dressler 1980). The importance of environment and the idea of transformation of galaxies in dense environments arose when Butcher & Oemler (1978) discovered that galaxy clusters at higher redshift contain a population of blue galaxies which nearby galaxy cluster counterparts are missing. However, it is still a matter of debate, which properties correlate with the decrease of blue galaxies from high- to low-redshift galaxy clusters, e.g. X-ray luminosity (Andreon & Etori 1999; Fairley et al. 2002), richness (Margoniner et al. 2001; De Propris et al. 2004), cluster concentration (Butcher & Oemler 1984; De Propris et al. 2004), presence of substructure (Metevier et al. 2000), cluster velocity dispersion (De Propris et al. 2004). Lewis et al. (2002) and Gómez et al. (2003) discuss the correlation between star formation rate and local projected density. The authors find low star formation rates at 2-3 virial cluster radii – which is equivalent to poor galaxy group densities. Therefore, galaxies may be preprocessed in groups, as physical processes in the studied clusters can not solely account for the observed variations in galaxy properties. Galaxy transformation as a smooth function of environment is also suggested by Cappellari et al. (2011) in terms of a *kinematic* morphology-density relation, i.e. separation into fast and slow rotators.

There have been a number of studies on the effect of environment on the H I content of galaxies in clusters (e.g. Giovanelli & Haynes 1985, Solanes et al. 2001, Gavazzi et al. 2005, Chung et al. 2009), and loose groups (e.g. Kilborn et al. 2005; Omar & Dwarakanath 2005). Through observations of isolated galaxies, we can define the expected H I mass in normal spiral galaxies of a particular linear optical diameter and morphological type. In dense regions, such as clusters, there is often an H I deficiency observed, indicating that H I gas is removed from galaxies in these environments (e.g. Solanes et al. 2001). Recent observations have found a similar H I deficiency in the less dense group environments (Omar & Dwarakanath 2005, Kilborn et al. 2009) indicating that the spirals may begin to lose their H I reservoir well before reaching the dense centre of a cluster.

An ideal target to study the effect of environment on the evolution of gas-rich galaxies, is the nearby Ursa Major cluster and its surroundings as most of the known member galaxies are late-type galaxies. The Ursa Major cluster is quite different in its nature compared to the well-known and similarly distant Virgo and Fornax clusters. Generally clusters are composed of hundreds of gas-poor early-type galaxies clustered around a central larger el-

liptical (e.g. Dressler 1980). The Ursa Major cluster is smaller – Tully et al. (1996) identified 79 high-probability cluster members. The cluster is essentially composed of late-type galaxies, in particular spiral galaxies with normal gas content, that are not centrally concentrated (Tully et al. 1996). This lack of a concentration towards any core and the overlap with many groups nearby the cluster might explain why the Ursa Major cluster is less studied compared to the Virgo and Fornax clusters. The several groups nearby the Ursa Major cluster make studying its dynamics a complex problem and the cluster difficult to define (Appleton & Davies 1982, Tully et al. 1996). However, Tully et al. (1996) define the cluster members to lie within a projected  $7.5^\circ$  circle centered at  $\alpha = 11^h56.9^m, \delta = +49^\circ22'$  and with heliocentric velocities between 700 and 1210 km s<sup>-1</sup>.

The cluster lies at a distance of 17.1 Mpc (Tully et al. 2008). The few previous studies of the Ursa Major cluster have found that it has a low velocity dispersion of only 148 km s<sup>-1</sup>, a virial radius of 880 kpc (Tully et al. 1996) and no X-ray emitting intra-cluster gas has yet been detected (Verheijen & Sancisi 2001). The Ursa Major cluster has a total mass of  $4.4 \times 10^{13} M_\odot$  (Tully 1987) and a B-band absolute luminosity of  $5.5 \times 10^{11} L_\odot$  (Tully et al. 2008). Compared to the Virgo cluster this is about 30 per cent of its light but only 5 per cent of its mass (Tully 1987, Tully et al. 2008). The number of H I-rich galaxies in Ursa Major is comparable to those in Virgo (Tully et al. 1996) and the Ursa Major cluster almost meets the Abell richness 0 standard. To qualify as an Abell richness class 0 the criteria are (i) 30 galaxies in B or (ii) 26 in R within 2 mag of the third brightest galaxy. The Ursa Major cluster is slightly short - 29 galaxies in B and 25 in R (Tully et al. 1996). Besides Ursa Major, only the Virgo cluster has such a high abundance of H I-rich galaxies on a 2 Mpc-scale in the nearby Universe ( $cz < 3000$  km s<sup>-1</sup>) (Tully et al. 1996).

Zwaan et al. (1999) note that the mostly late-type galaxies in the Ursa Major cluster do not seem to be seriously affected by tidal interactions indicating that the system is in an *early evolutionary state*. However, Verheijen & Sancisi (2001) studied 43 spiral galaxies in detail and found 10 interacting systems that show distorted morphologies and tidal debris. There is a deficiency of known dwarf galaxies in the Ursa Major cluster – there are only two dozen dwarfs, whereas up to  $10^3$  could be expected to be found if the same steep luminosity function claimed for Virgo was valid for the Ursa Major cluster (Trentham et al. 2001). To date, (i) the small number of dwarf galaxies, (ii) the low velocity dispersion, (iii) the non-detection of X-ray emitting intra-cluster gas, (iv) the low abundance of elliptical galaxies in the cluster and (v) the total mass  $< 10^{14} M_\odot$  challenge the question “why not call it a group?”. Clusters usually have a broader velocity distribution, a hot intra-cluster gas which can strip the galaxies off their H I gas and an enhanced population of both the early-type (S0 and E) galaxies and the H I depleted spiral galaxies. As the majority of the Ursa Major members are H I-rich spiral galaxies such as those one finds in the field, the distinction between the ‘Ursa Major cluster’ as opposed to an ‘Ursa Major group’ isn’t clear. One hypothesis is that Ursa Major is a *newly forming cluster* given that the estimated crossing time is approximately half a Hubble time, in contrast to Virgo and Fornax where the crossing times are 0.08 and 0.07  $H_0^{-1}$ , respectively (Tully et al. 1996).

In this paper we present the catalogue of H I sources as detected in the first blind H I survey of the Ursa Major region (approximately 480 deg<sup>2</sup>). The analyzed region overlaps with the

<sup>1</sup> <http://www.atnf.csiro.au/research/WALLABY/proposal.html>

Canes Venatici region for which Kovač et al. (2009) have conducted a deep blind HI survey (HI mass sensitivity  $\sim 10^6 M_\odot$ ) using the Westerbork Synthesis Radio Telescope (WSRT) in an area of  $86 \text{ deg}^2$  ( $v_{\text{sys}} \leq 1330 \text{ km s}^{-1}$ ). Our HI data were obtained as part of the HI Jodrell All Sky Survey (HIJASS). The data acquisition and determination of the HI sources are described in Section 2 including a discussion of the catalogue completeness and reliability. The HI properties of the sources are presented in a catalogue in Section 3. The HI mass limit of the presented catalogue is  $2.5 \times 10^8 M_\odot$  assuming a velocity width of  $100 \text{ km s}^{-1}$  and a distance of  $17.1 \text{ Mpc}$ . First results and basic property distributions of the HIJASS sources are presented in Section 4. Furthermore, we identify galaxy pairs/systems that are high-probability candidates for galaxy-galaxy interactions and discuss four systems in detail, two of which show strikingly extended HI content.

In a forthcoming paper we will investigate the nature of the Ursa Major cluster/group and probe the hypothesis that it is a *newly forming cluster*. We will study substructures and their dynamics, and present dynamical masses, total mass-to-light ratios etc. for both individual galaxies and the subregions. Furthermore, to investigate the HI properties of galaxies residing in different density regions, we will analyze the HI sources in the Ursa Major cluster and compare them to galaxies residing in foreground groups and the less dense filament connecting the Ursa Major with the Virgo cluster, which lies south of Canes Venatici.

## 2 OBSERVATIONS AND DATA ANALYSIS

### 2.1 Data acquisition and processing

The HI data cubes analyzed in this paper were obtained in 2001–2002 as part of the HI Jodrell All Sky Survey (HIJASS) (Lang et al. 2003). The blind HI survey was conducted using the 4-beam receiver mounted on the 76.2-m Lovell telescope at Jodrell Bank observatory, UK. HIJASS covered more than  $1000 \text{ deg}^2$  in the northern sky ( $\delta \geq +22^\circ$ ) complementary to (i) the HI Parkes All Sky Survey (HIPASS) which surveyed the entire southern sky ( $\delta \leq +2^\circ$ ) from 1997 to 2000 (Staveley-Smith et al. 1996; Barnes et al. 2001; Koribalski et al. 2004) and (ii) the northern extension to HIPASS ( $+2^\circ \leq \delta \leq +25^\circ 30'$ ) carried out in 2000 to 2002 (Wong et al. 2006). HIJASS provides the first blind HI survey of the nearby Ursa Major cluster and its surroundings. To investigate the Ursa Major region we only consider velocities in the range  $300$  to  $1900 \text{ km s}^{-1}$  (all velocities are given in the optical convention  $cz$ ). Sources with systemic velocities below  $300 \text{ km s}^{-1}$  are excluded to minimize confusion with high-velocity clouds and Galactic emission – an exception are 15 obviously real galaxies with systemic velocities between  $150$  and  $300 \text{ km s}^{-1}$  that are included in the catalogue. We note that HIJASS data suffers from a broad band of radio-frequency interference between  $4500$  and  $7500 \text{ km s}^{-1}$  (Lang et al. 2003), which lies outside our studied velocity range.

The Ursa Major region is covered by seven HIJASS data cubes measuring  $8^\circ \times 8^\circ$  and one HIJASS cube measuring  $5^\circ \times 8^\circ$  in size (the sky coverage is approximately  $480 \text{ deg}^2$ ). The cubes span a range in right ascension (RA) between  $10^h 45^m$  and  $13^h 04^m$  and a range in declination (Dec.) between  $22^\circ$  and  $54^\circ$ . We note that the analyzed region overlaps with the Canes Venatici region for which Kovač et al. (2009) have conducted a deep blind HI survey in an area of  $86 \text{ deg}^2$  ( $v_{\text{sys}} \leq 1330 \text{ km s}^{-1}$ ). The HIJASS

**Table 1.** The peak and integrated correction factors ( $f_p$  and  $f_{\text{int}}$ ) for extended sources as a function of FWHM ( $x$ ).

$$f(x) = a_3 x^3 + a_2 x^2 + a_1 x + a_0$$

Coefficient	$f_p(x)$	$f_{\text{int}}(x)$
$a_3$	$-4.78 \times 10^{-6}$	$7.12 \times 10^{-6}$
$a_2$	$5.54 \times 10^{-4}$	$-2.27 \times 10^{-4}$
$a_1$	$-2.26 \times 10^{-2}$	$1.05 \times 10^{-2}$
$a_0$	1.112	1.003

cubes have a spatial pixel size of  $4 \times 4 \text{ arcmin}^2$ . In the third dimension, the channel spacing is  $62.5 \text{ kHz}$  which corresponds to an increment of  $13.2 \text{ km s}^{-1}$  at the rest frequency of HI. The velocity resolution is  $18 \text{ km s}^{-1}$  after smoothing to reduce ‘ringing’ caused by Galactic emission (applying 25 per cent Tukey filter). The root mean square (rms) noise level in the analyzed data is  $12\text{--}14 \text{ mJy beam}^{-1}$ . To minimize edge effects the overlapping HIJASS data cubes are mosaiced to one mega-cube. For further information on data reduction, the Lovell telescope and HIJASS see Lang et al. (2003).

The angular resolution of the Lovell telescope at  $1.4 \text{ GHz}$  is  $12.0 \text{ arcmin}$  (Lang et al. 2003). The gridding process (using similar parameters as for HIPASS) slightly degrades the angular resolution (see Barnes et al. 2001). According to Barnes et al. (2001) the resultant beam size is not well-defined and depends on smoothing radius, pixel size, source position, shape and strength (signal-to-noise ratio) as the gridding is a non-linear process. One can only assess the gridded beam size by analysing simulations and synthetic source injections. To determine the gridded beam size, we inject synthetic point sources into the raw data and measure their properties after the gridding process. We determine the full width at half-maximum beamwidth (FWHM) of a two-dimensional Gaussian fit to the synthetic sources, analogous to Barnes et al. (2001). The measured beamwidths vary as a function of source peak brightness (in  $\text{Jy beam}^{-1}$ , which corresponds to  $\text{Jy}$  for point sources). Given a wide range of peak flux densities in the presented catalogue – the majority of sources have  $33 \leq S_p \leq 300 \text{ mJy}$  and a few strong sources range to  $3.5 \text{ Jy}$  in peak flux density – we determine two appropriate beamwidths: (i)  $13.1 \pm 0.9 \text{ arcmin}$  for the majority of sources with  $S_p \leq 300 \text{ mJy}$  and (ii)  $12.4 \pm 0.6 \text{ arcmin}$  for sources with  $S_p > 300 \text{ mJy}$ .

The peak and integrated fluxes of point sources are preserved during the gridding process but for extended sources, the peak and integrated fluxes require a correction: We calculated the correction factors by similarly injecting synthetic extended sources into the raw data and measure their properties after the gridding process (analogous to Barnes et al. 2001). The correction factors for extended sources as a function of FWHM are given in Table 1. We obtain this function by fitting a third order polynomial to the median data points (with  $R^2$  of 99.9%). In our catalogue (Section 3.2), we quote both the measured and corrected fluxes for extended sources.

## 2.2 Data analysis using DUCHAMP

We use the automated source finder DUCHAMP-1.1.8 (Whiting 2012)<sup>2</sup> on the H I data cube to compile our initial candidate galaxy list. DUCHAMP is based on a threshold method and searches for groups of adjacent pixels in position and velocity that are above the given threshold, which is estimated from the cube statistics (in Jy beam<sup>-1</sup>) or alternatively specified from the user as a peak flux density value. Furthermore the user can (i) reduce the noise prior to the searching via wavelet reconstruction and/or smoothing (spatial or spectral) and (ii) control various parameters such as the minimum extent of the detections in pixels and/or channels. DUCHAMP provides a list of the H I detections and their properties, the H I spectra and integrated H I intensity maps (moment zero). The DUCHAMP outputs need to be inspected carefully as H I sources are occasionally merged. We can identify such sources by eye and separate them when they do not overlap both spatially and spectrally.

We made a comprehensive test of various input parameters and methods to facilitate DUCHAMP detections of low peak flux and extended H I sources without disproportionately increasing noise detections (see Section 2.3 and 2.5). We first apply a spectral Hanning smoothing to the HIJASS data and then reconstruct them with the ‘à trous’ wavelet method. Hanning smoothing correlates neighbouring pixels in the spectral domain and determines the weighted average flux over a certain number of channels – the channel spacing remains 13.2 km s<sup>-1</sup>. We determine that the optimal Hanning smoothing width for the data is seven channels (see Section 2.3). The wavelet method reconstructs each spectrum separately and we chose the following criteria when compiling the DUCHAMP detection list: (i) the detection must be contiguous in two channels and (ii) the peak flux density of the candidate galaxies must be above 16 mJy. This is an approximate 2.5 $\sigma$  peak flux density threshold as the mean noise level in the smoothed and reconstructed cube is  $\sim 6.6$  mJy beam<sup>-1</sup>.

In this paper, we only consider 5 $\sigma$  detections in peak flux in the edge-masked HIJASS megacube to present a reliable and complete catalogue of H I sources in the Ursa Major region within 300 to 1900 km s<sup>-1</sup>. This corresponds to a minimum in peak flux density of 33 mJy and an H I mass limit of  $2.5 \times 10^8 M_{\odot}$  (assuming a velocity width of 100 km s<sup>-1</sup> and a distance of 17.1 Mpc). These selection criteria lead to a DUCHAMP detection list with 140 candidate galaxies including merged detections (doubles to quads) that are labelled in Section 3.2.

## 2.3 Catalogue reliability – Negative troughs

To test the reliability of the 5 $\sigma$  peak flux DUCHAMP detection list, we investigate the negative troughs in the edge-masked HIJASS cube. When using the selection criteria as discussed in Section 2.2, we identify 25 negative troughs with  $S_p \leq -33$  mJy and  $w_{50} \geq 26.4$  km s<sup>-1</sup>. All 25 negative troughs can be associated with negative bandpass sidelobes, i.e. an artifact of bandpass removal which is apparent north and south of strong H I sources (see e.g. Barnes et al. 2001). This lack of negative detections (noise peaks) indicates that the positive DUCHAMP candidate galaxy list with  $S_p \geq 33$  mJy and  $w_{50} \geq 26.4$  km s<sup>-1</sup> contains high-probability real H I sources.

Hanning smoothing is known to enhance the brightness of sources – on the scale of the smoothing width – with respect to the noise in each channel map, but reduces the peak strength (signal-to-noise) of sources on other scales. Whiting (2012) shows that an appropriately chosen smoothing width can still increase the recovery rate of sources on different scales than the smoothing width as the noise level is suppressed. However, to prevent loss of information on different scales, we also use the wavelet reconstruction to further suppress the noise and to enhance structures on various scales (narrow and broad profiles). Using wavelet reconstruction also suppresses noise peaks, baseline ripples or radio-frequency interferences as discussed in Westmeier et al. (2011). For further information on DUCHAMP and the noise suppression methods see Whiting (2012).

Some restrictions on spatial and spectral extent of DUCHAMP detections greatly improve the reliability, such as the applied minimum number of channels ( $\geq 2$ ) in which the detection must be contiguous (Whiting 2012). The selection criteria as listed in Section 2.2 are chosen to limit the number of false detections and to present a reliable catalogue of H I sources in the Ursa Major region in this paper.

## 2.4 Catalogue reliability – Follow-up observations

The reliability of the catalogue is increased by follow-up observations and rejection of unconfirmed sources from the catalogue. We re-observed 17 apparent first time detections in HIJASS with the Green Bank Telescope (GBT, FWHM 9 arcmin) – nine of which have an associate optical counterpart that match in position and velocity to the H I detection and eight candidate galaxies/H I clouds without a previously catalogued optical counterpart. The rms noise level is between 4 and 7 mJy for H I sources with an associate optical counterpart and approximately 3 mJy for the candidate galaxies/H I clouds. Given that the lowest peak flux density of the candidate galaxies/H I clouds is 33 mJy, this will lead to signal-to-noise detections  $> 10$ . The velocity resolution of the GBT data is 3.3 km s<sup>-1</sup> after boxcar smoothing.

The GBT follow-up observations confirmed all nine H I sources with an associate optical counterpart. However, only one out of the eight candidate galaxies/H I clouds was confirmed, namely HIJASS J1219+46. Therefore, 7 initial DUCHAMP detections are excluded from the presented catalogue in this paper. Inspecting the original as well as the smoothed and reconstructed data cubes by eye reveal that the unconfirmed detections are noise peaks on top of large-scale baseline ripples. DUCHAMP provides an option ‘flag baseline’ which removes the baseline from each spectrum prior to compiling the detection list. However, we did not utilize this option as not only does it remove all candidate galaxies/H I clouds from the detection list, some of the faint H I detections with an associate optical counterpart were not included as well.

## 2.5 Catalogue completeness – Synthetic source injection

To measure the catalogue completeness we insert numerous synthetic point sources into the eight HIJASS cubes, prior to running DUCHAMP. The rate at which the synthetic sources are recovered reflects the completeness, as discussed explicitly in Zwaan et al. (2004) (also see Wong et al. 2006). The criteria for a recovered synthetic source are a DUCHAMP detection within 10 arcmin

<sup>2</sup> <http://www.atnf.csiro.au/people/Matthew.Whiting/Duchamp>

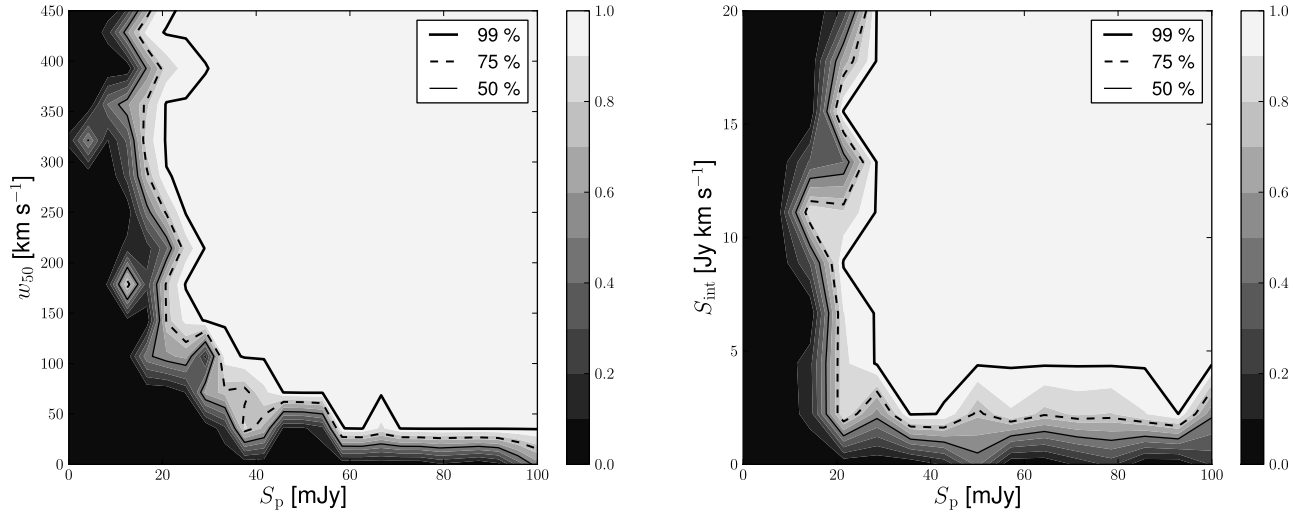


**Figure 1.** The DUCHAMP completeness in a representative HIJASS cube as a function of  $S_p$  and  $w_{50}$  (left) and as a function of  $S_p$  and  $S_{\text{int}}$  (right). The brighter colours correspond to high completeness levels and the contour lines show the 99, 75 and 50 per cent completeness levels.

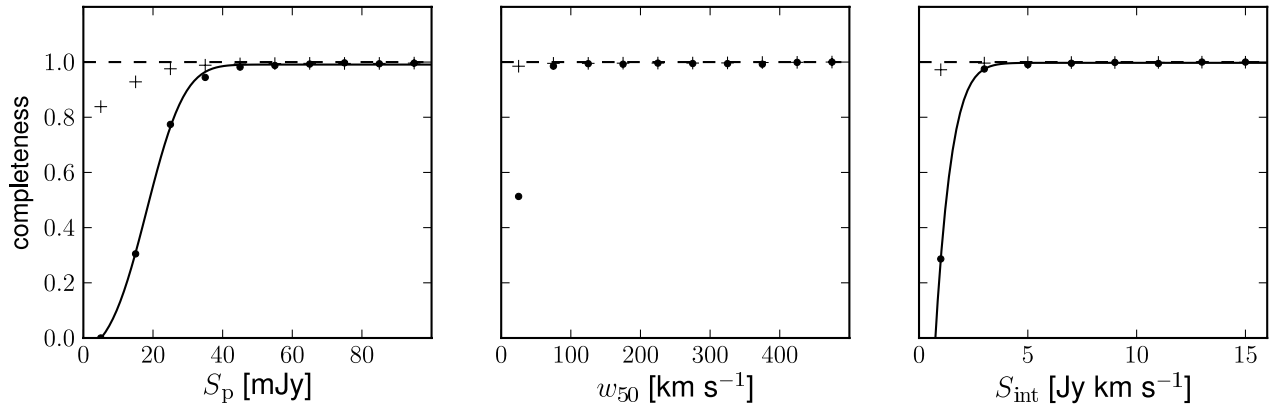


**Figure 2.** The DUCHAMP completeness as a function of  $S_p$ ,  $w_{50}$  and  $S_{\text{int}}$ . The differential completeness is marked with circles whereas the cumulative completeness is marked with crosses. The solid lines are the error function fits to the data.

and  $200 \text{ km s}^{-1}$  of the original position and velocity of the synthetic source (the average position and velocity accuracies for HI sources with peak flux densities below  $100 \text{ mJy}$  are  $\sim 1.2 \text{ arcmin}$  and  $\sim 14 \text{ km s}^{-1}$ , respectively).

The synthetic point sources are given a Gaussian spectral shape and have random positions, 50 per cent velocity widths and peak flux densities (Kilborn et al. 2009). The 50 per cent velocity widths are  $w_{50} \leq 500 \text{ km s}^{-1}$  and the peak flux densities are  $S_p \leq 100 \text{ mJy}$ . The synthetic sources are placed away from the noisy edges of the data cube and are not placed on top of other sources either synthetic or real (the positions of the real sources are according to an initial DUCHAMP output list).

A total of 2000 synthetic sources are inserted into each HIJASS data cube to obtain the DUCHAMP completeness. For a representative HIJASS cube the completeness is shown in Figure 1. We use natural neighbor interpolation to achieve the grey-scale

representation of the completeness depending on  $S_p$  and  $w_{50}$  or  $S_p$  and integrated flux  $S_{\text{int}}$  (which is a combination of both  $S_p$  and  $w_{50}$ ).

To measure the catalogue completeness as a function of one parameter only -  $S_p$ ,  $w_{50}$  or  $S_{\text{int}}$  - we integrate along the other variable of the completeness as discussed in Zwaan et al. (2004). We integrate above the DUCHAMP selection parameters which are  $w_{50} = 26.4 \text{ km s}^{-1}$  and  $S_p = 16 \text{ mJy}$ . These values mark the DUCHAMP detection limit in the smoothed and reconstructed cube - below these values the completeness drops to zero. Figure 2 shows this differential completeness (circles) as well as the cumulative (crosses) completeness as defined by Zwaan et al. (2004). Figure 2 also shows the error function fit to the data to determine the 95 per cent confidence levels which lie at  $S_p = 33 \text{ mJy}$  and  $S_{\text{int}} = 2.63 \text{ Jy km s}^{-1}$ . The 99 per cent completeness levels are achieved at  $S_p = 45 \text{ mJy}$  and  $S_{\text{int}} = 3.55 \text{ Jy km s}^{-1}$ . Therefore,

the peak flux density limited catalogue (at 33 mJy) presented in Section 3 is 95 per cent complete.

## 2.6 Catalogue completeness – Literature comparison

As an additional measure of completeness we compare our results (Section 3.2) to an overlapping deep blind H I survey in the Canes Venatici region using WSRT (area of 86 deg<sup>2</sup>,  $v_{\text{sys}} \leq 1330$  km s<sup>-1</sup> with an H I mass sensitivity of  $\sim 10^6$  M<sub>⊙</sub>; Kovač et al. 2009). We find that our presented catalogue contains all but one H I sources in the velocity range 300 to 1330 km s<sup>-1</sup>, with  $S_p \geq 33$  mJy and  $S_{\text{int}} \geq 2.63$  Jy km s<sup>-1</sup> (95 per cent completeness level) as listed in Kovač et al. (2009) – the exception is NGC4460 ( $v_{\text{LG}} = 542$  km s<sup>-1</sup>) with  $S_p = 41$  mJy and  $S_{\text{int}} = 4.30$  Jy km s<sup>-1</sup> (Kovač et al. 2009). We investigated the HIJASS data cube (by eye) and identify NGC4460 at the end of negative bandpass sidelobes emerging from the strong double source NGC4490/NGC4485. NGC4460 has reduced peak brightness ( $S_p \approx 31$  mJy beam<sup>-1</sup>) due to the negative bandpass sidelobes, which prevents this H I source to be listed in our catalogue. We conclude that negative bandpass sidelobes may cause a deficit in completeness for sources with  $16 \leq S_p \leq 45$  mJy and  $w_{50} \leq 100$  km s<sup>-1</sup> (see Figure 1), as their peak flux densities may lie below the detection threshold. However, this is a small effect, given the little area affected by negative bandpass sidelobes.

## 3 THE HI CATALOGUE

### 3.1 Parametrization

The sources found using DUCHAMP are parameterized with an interactive script utilising the MIRIAD software package (Sault et al. 1995). The parametrization is necessary as DUCHAMP gives initial values – dealing with double detections and obtaining reliable H I parameters requires user input. Our method is similar to Lang et al. (2003) and Koribalski et al. (2004) and this will be briefly described in the following section.

A spatially integrated spectrum is generated from the original HIJASS cube, using the DUCHAMP output parameters for each source (RA, Dec., velocity, velocity widths). The spectral extent of the H I source (velocity range) can be adjusted as necessary. An integrated H I intensity map over this velocity range is generated using the MIRIAD task MOMENT. Given a specified fitting area (in relation to the source size), IMFIT is used to determine the central position of the H I source by fitting a two-dimensional Gaussian to the integrated H I intensity map. The obtained central coordinates are used to generate a new spatially integrated spectrum weighted according to the extent of the H I source (see below). In general, we fit and subtract a first-order baseline fit to the spectrum (higher order baseline fits are labelled in the catalogue). The H I parameters such as peak and integrated flux, the velocity widths, the clipped rms noise and the systemic velocity are measured using MBSPECT. In the catalogue we quote the integrated flux measured with the robust moments, the 20 and 50 per cent velocity widths calculated from the width maximiser and the systemic velocity as the center of the 20 per cent velocity width (see Meyer et al. 2004 for definitions).

An H I source can be unresolved or extended with respect to the gridded beam size. To identify point and extended sources, we compare the integrated flux measurements obtained from (i)

spectra where every pixel is weighted according to the expected beam response (beam-weighted as for point sources) to (ii) spectra where the flux is directly summed (as for extended sources). The considered area is given by a box surrounding the central position, e.g. of size  $5 \times 5$  pixel<sup>2</sup> or  $7 \times 7$  pixel<sup>2</sup> that correspond to  $20' \times 20'$  and  $28' \times 28'$ , respectively. A potentially extended source is identified due to an increase in the integrated flux from a beam-weighted spectrum to a summed spectrum in a bigger box. This increase can also occur due to confusion with a nearby H I source which might be included in the bigger box - such sources are flagged as double sources (d) in the catalogue and are parameterized by generating a beam-weighted spectrum as for point sources. Truly extended sources (e), which are indicated by an increase in the integrated flux, are confirmed by investigating the residual map of the Gaussian fit. An extended source will show flux in the residual map whereas a point source is well described by the Gaussian fit.

### 3.2 The HI catalogue

The DUCHAMP detection list in the smoothed and reconstructed HIJASS megacube contains 140 candidate galaxies with systemic velocities between 300 and 1900 km s<sup>-1</sup>. After the parametrization process, 4 galaxies have systemic velocities below 300 km s<sup>-1</sup>. In addition, we identified 11 H I sources with systemic velocities between 150 and 300 km s<sup>-1</sup> that are included in the sample as they are obviously real galaxies as opposed to Galactic emission or high-velocity clouds. However, H I sources with systemic velocities below 300 km s<sup>-1</sup> are not included in Section 4. Furthermore we identified several double, triple and quad detections that are separated during the parametrization process leading to a total of 173 H I sources that are parameterized from the original HIJASS megacube. We exclude 7 detections from the presented catalogue that are unconfirmed in GBT follow-up observations (see Section 2.4). Therefore a total of 166 H I sources are listed in our catalogue in Section 3.2.

The parameterized H I sources are cross-correlated with galaxies listed in the NASA/IPAC Extragalactic Database (NED; as of September 2012) and the Sloan Digital Sky Survey (SDSS DR8). We only consider galaxies with cross-identifications in NED and galaxies with spectroscopic redshifts with confidence levels  $z_{\text{conf}} > 0.95$  in SDSS as possible counterparts. We associate an H I source with a catalogued galaxy, if this galaxy is within the gridded beam size (or within the extent of the H I intensity contours for large sources) and within the velocity range of the H I source. We find 54 H I sources that have multiple candidate counterparts. These are potentially confused H I sources and may be interacting systems. To determine the most likely optical counterpart (listed in the first row of the catalogue), the H I position uncertainty, the heliocentric velocity, the optical galaxy size (in relation to the H I mass and size) and the morphology are considered.

We find only one out of the 166 catalogued H I sources that does not have an associate optical counterpart listed in NED/SDSS or visible on Palomar Digitized Sky Survey (DSS) images. This candidate galaxy/H I cloud – HIJASS J1219+46 – is discussed in Section 3.4.

Table 2 lists the H I sources and their optical counterparts as follows: column (A1) gives the HIJASS name; columns (A2)–(A4) list the central H I position (RA [J2000], Dec. [J2000]) and its uncertainty  $\sigma_{\text{pos}}$  (all uncertainties are discussed in Section 3.3); column (A5) contains the systemic velocity (km s<sup>-1</sup>)

with its uncertainty  $\sigma_v$ ; column (A6) states ‘ID’ for H I detections that have an optical identification and ‘PUO’ for the previously uncatalogued gas-rich object; columns (A7)–(A10) list the details of the optical counterparts, i.e. name, RA (J2000), Dec. (J2000) and heliocentric velocity ( $\text{km s}^{-1}$ ); columns (A11) and (A12) give the angular separation (arcmin) and velocity offset ( $\text{km s}^{-1}$ ) from the H I parameters. The most likely optical counterpart is given in the first row and galaxies that lie within the gridded beam or within the extent of the H I intensity contours (for large sources) and might confuse the H I content are quoted in the subsequent rows.

The measured H I properties of the HIJASS detections are given in Table 3. The columns are as follows: column (B1) gives the HIJASS name; columns (B2)–(B4) gives the measured and corrected peak flux densities ( $S_p$ ) with its uncertainty (in Jy); columns (B5)–(B7) list the measured and corrected integrated flux ( $S_{\text{int}}$ ) with its uncertainty (in  $\text{Jy km s}^{-1}$ ); columns (B8) and (B9) contain the velocity widths at 50 and 20 per cent of the peak flux density with their uncertainties (in  $\text{km s}^{-1}$ ); column (B10) gives the clipped rms measured in MBSPECT; column (B11) lists the distance to the galaxy (in Mpc) as obtained from the Extragalactic Distance Database (EDD; Tully et al. 2009 – only distances obtained from Color-Magnitude Diagrams, Tip of the Red Giant Branch and other high quality methods are considered) or calculated from the local group velocity (see Koribalski et al. 2004 for HIPASS) – we adopt  $H_0 = 70 \text{ km s}^{-1} \text{ Mpc}^{-1}$ ; for galaxies within the cluster definition by Tully et al. (1996) we adopt a distance of 17.1 Mpc; column (B11) gives the logarithm of the H I mass and column (B12) contains flags for 78 extended (e) and 54 confused (c) H I sources, 38 H I sources which are part of DUCHAMP double detections (d), 10 H I sources without a central position from a position fit (f) and therefore without major/minor axis measurements, 10 H I sources lying nearby negative bandpass sidelobes (b), 10 newly detected H I sources in the 21-cm emission line (n), 15 H I sources with systemic velocities below  $300 \text{ km s}^{-1}$  (v), 34 sources where independent distance measurements are available (i) and numbers to indicate higher order baseline fits. The H I mass in column (B11) is calculated from the integrated flux ( $S_{\text{int}}$  and  $S_{\text{int}}(\text{corr})$  for extended sources respectively) according to  $M_{\text{HI}} = 2.356 \times 10^5 \times D^2 \times S_{\text{int}} [\text{M}_\odot]$  with distances as given in column (10). We note that Kovač et al. (2009) also determine adequate distances in the local group frame, neglecting peculiar velocities (using Yahil et al. 1977).

We show a velocity integrated H I map with symbols marking the projected positions of all parameterised H I sources in this catalogue in Figure 3. H I sources with an associated optical counterpart are marked with open ellipses whereas the previously uncatalogued H I source is marked with a filled ellipse (black). Furthermore previously catalogued sources that are newly detected in H I are marked with crosses. The size of the ellipses indicate the measured major axis – ellipses surrounded by boxes mark H I detections for which no central position and no extent (major and minor axis) is measurable (usually weak H I sources or double detections for which we retain the position of the optical counterpart). The projected position of the Ursa Major cluster as defined by (Tully et al. 1996) is overlaid with a large circle.

### 3.3 HI parameter uncertainties

In Table 2 and 3 we give several uncertainties of measured H I parameters which are calculated as follows:

The position uncertainty is derived from the gridded beam size ( $FWHM$ ) and the H I signal-to-noise (Koribalski et al. 2004):

$$\sigma_{\text{pos}} = \frac{FWHM}{S_p/rms}$$

This individual position uncertainty is considered when determining the most likely optical counterpart (see Table 2).

The peak flux uncertainty strongly depends on the rms noise for weak sources and to a lesser degree on the peak flux (see Barnes et al. 2001). The formula we use is analogous to the one in HIPASS (Koribalski et al. 2004), which is as follows:

$$\sigma_{\text{peak}}^2 = rms^2 + (0.05S_p)^2$$

The uncertainty in integrated flux is calculated as discussed in Koribalski et al. (2004) whereby

$$\sigma_{\text{int}} = 4 \times \left(\frac{S_p}{rms}\right)^{-1} \times (S_p \times S_{\text{int}} \times R)^{0.5}$$

with  $R=18.1 \text{ km s}^{-1}$ , which is the velocity resolution of the HIJASS data.

The systemic velocity uncertainty is

$$\sigma_v = 3 \times \left(\frac{S_p}{\sigma_{\text{peak}}}\right)^{-1} \times (R \times 0.5(w_{20} - w_{50}))^{0.5}$$

as discussed in Koribalski et al. (2004).

The uncertainties in the 50% and 20% velocity widths are:

$$\sigma_{50} = 2 \times \sigma_v$$

$$\sigma_{20} = 3 \times \sigma_v$$

as discussed in Fouqué et al. (1990).

Table 2: The HIJASS detections and possible optical counterparts.

HIJASS name (A1)	RA (J2000.0) (A2)	Dec. (J2000.0) (A3)	$\sigma_{\text{pos}}$ arcmin (A4)	$v_{\text{sys}} \pm \sigma_v$ km s <sup>-1</sup> (A5)	Class (A6)	NED ID <sup>a,b</sup> (A7)	RA (J2000.0) (A8)	Dec. (J2000.0) (A9)	vel. km s <sup>-1</sup> (A10)	pos. & vel. offsets arcmin (A11)	pos. & vel. offsets km s <sup>-1</sup> (A12)
HIJASS J11048+46	10:48:43.33	46:43:10.0	2.7	741 ± 6	ID	UGC05917	10:48:53.73	46:43:14.6	741	1.8	0
HIJASS J1054+49	10:54:57.73	49:42:53.6	2.9	1347 ± 15	ID	UGC06029	10:55:02.23	49:43:33.1	1363	1.0	16
-	-	-	-	-	-	J105502.69+494340.9	10:55:02.70	49:43:40.9	1357	1.1	10
HIJASS J1102+52	11:02:48.05	52:06:40.5	2.0	949 ± 7	ID	UGC06113	11:02:47.85	52:06:48.8	951	0.1	2
HIJASS J1108+53	11:08:08.79	53:36:41.6	2.1	1226 ± 6	ID	UGC06182	11:08:03.01	53:36:57.6	1238	0.9	12
-	-	-	-	-	-	J110801.86+533702.7	11:08:01.87	53:37:02.7	1176	1.1	50
-	-	-	-	-	-	J110819.94+533627.7	11:08:19.94	53:36:27.8	1087	1.7	139
HIJASS J1109+50	11:09:32.53	50:56:24.0	1.6	906 ± 7	ID	UGC06202	11:09:36.50	50:55:36.3	920	1.0	14
HIJASS J1110+46	11:10:00.51	46:05:03.1	1.9	1409 ± 6	ID	UGC06205	11:09:58.36	46:05:41.6	1414	0.7	5
HIJASS J1113+53	11:13:22.74	53:35:25.9	0.5	927 ± 2	ID	UGC06251	11:13:26.14	53:35:42.3	927	0.6	0
-	-	-	-	-	-	J111343.60+533848.3	11:13:43.61	53:38:48.3	914	4.6	13
HIJASS J1120+53	11:20:59.85	53:09:48.4	0.3	1156 ± 2	ID	NGC3631	11:21:02.88	53:10:10.5	1156	0.6	0
-	-	-	-	-	-	J112059.33+531125.7	11:20:59.33	53:11:25.8	1192	1.6	36
-	-	-	-	-	-	J112110.21+530951.5	11:21:10.21	53:09:51.5	1073	1.6	83
HIJASS J1123+50	11:23:14.03	50:53:42.2	2.7	793 ± 7	ID	UGC06399	11:23:23.22	50:53:33.8	791	1.5	2
HIJASS J1123+52	11:23:53.92	52:54:51.2	0.6	1213 ± 3	ID	NGC3657	11:23:55.58	52:55:15.6	1215	0.5	2
HIJASS J1126+53	11:26:41.09	53:44:23.3	0.9	646 ± 3	ID	UGC06446	11:26:40.46	53:44:48.0	644	0.4	2
HIJASS J1132+53	11:32:35.89	53:03:19.0	0.5	994 ± 3	ID	NGC3718	11:32:34.85	53:04:04.5	993	0.8	1
-	-	-	-	-	-	NGC3729	11:33:49.32	53:07:32.0	1060	11.8	66
HIJASS J1132+39	11:32:44.58	39:04:53.5	1.7	1557 ± 7	ID	UGC06531	11:32:49.21	39:05:05.6	1565	0.9	8
HIJASS J1133+47	11:33:20.68	47:01:22.5	0.6	863 ± 3	ID	NGC3726	11:33:21.12	47:01:45.2	866	0.4	3
-	-	-	-	-	-	J113318.79+470338.5	11:33:18.79	47:03:38.5	779	2.3	84
-	-	-	-	-	-	J113314.01+470226.0	11:33:14.01	47:02:26.0	869	1.6	6
HIJASS J1136+45	11:36:04.30	45:16:54.2	0.2	230 ± 2	ID	NGC3741	11:36:06.18	45:17:01.1	229	0.4	1
HIJASS J1136+36	11:36:32.91	36:24:37.2	1.4	1569 ± 5	ID	NGC3755	11:36:33.37	36:24:37.3	1570	0.1	1
HIJASS J1137+47	11:37:42.72	47:53:14.5	0.6	733 ± 4	ID	J113654.64+362316.3	11:36:54.64	36:23:16.4	1591	4.6	22
-	-	-	-	-	-	NGC3769	11:37:44.11	47:53:35.1	737	0.4	4
-	-	-	-	-	-	NGC3769A	11:37:51.36	47:52:52.8	734	1.5	1
HIJASS J1138+35	11:38:00.28	35:12:55.5	1.8	1625 ± 8	ID	UGC06603	11:38:02.13	35:12:13.0	1635	0.8	10
HIJASS J1138+33	11:38:44.75	33:48:43.6	2.2	1847 ± 6	ID	UGC06610	11:38:44.16	33:48:20.8	1851	0.4	4
-	-	-	-	-	-	iJ1138440+334817 <sup>c</sup>	11:38:44.01	33:48:17.2	1880	0.5	33
HIJASS J1138+43	11:38:53.56	43:12:23.3	1.7	1205 ± 8	ID	UGC06611	11:38:51.55	43:09:51.8	1192	2.6	13
-	-	-	-	-	-	iJ1138515+430955 <sup>c</sup>	11:38:51.51	43:09:56.4	1141	2.5	64
HIJASS J1139+46	11:39:21.86	46:30:34.1	0.5	733 ± 3	ID	NGC3782	11:39:20.76	46:30:49.8	739	0.3	6
-	-	-	-	-	-	J11390927+4641152 <sup>c</sup>	11:39:09.23	46:41:14.6	836	10.9	103
-	-	-	-	-	-	J113948.69+463711.4	11:39:48.70	46:37:11.4	702	8.1	31
-	-	-	-	-	-	J113948.83+463711.6	11:39:48.83	46:37:11.6	612	8.1	121
HIJASS J1140+45	11:40:05.75	45:56:20.4	0.5	848 ± 2	ID	UGC06628	11:40:05.75	45:56:31.8	841	0.2	7
-	-	-	-	-	-	J114035.57+460727.5	11:40:35.58	46:07:27.6	843	12.3	5



Table 2 – Continued

HIJASS name (A1)	RA (J2000.0)		Dec. (J2000.0)		$\sigma_{\text{pos}}$ arcmin (A4)	$v_{\text{sys}} \pm \sigma_v$ km s <sup>-1</sup> (A5)	Class (A6)	NED ID <sup>a,b</sup> (A7)	RA (J2000.0)		Dec. (J2000.0)		vel. km s <sup>-1</sup> (A10)	pos. & vel. offsets arcmin (A11)	km s <sup>-1</sup> (A12)
	(A2)	(A3)	(A8)	(A9)					(A8)	(A9)					
HIJASS J1141+46	11:41:11.61	46:24:10.9	1.6	743 ± 5	ID	CGCG242-075	11:41:21.97	46:23:35.5	743	1.9	0				
HIJASS J1141+36	11:41:20.37	36:32:41.5	1.6	1467 ± 7	ID	NGC3813	11:41:18.66	36:32:48.5	1465	0.4	2				
HIJASS J1141+32	11:41:26.23	32:18:29.4	2.0	1820 ± 8	ID	MRK0746	11:41:29.86	32:20:59.5	1801	2.6	19				
-	-	-	-	-	-	KUG1138+327	11:41:07.49	32:25:37.2	1796	8.2	24				
-	-	-	-	-	-	WAS28	11:41:36.71	32:16:51.6	1769	2.8	51				
HIJASS J1142+51	11:42:22.40	51:33:35.0	2.3	986 ± 10	ID	UGC06667	11:42:26.29	51:35:52.7	973	2.4	13				
-	-	-	-	-	-	J114226.26+513552.6	11:42:26.26	51:35:52.6	1034	2.4	48				
HIJASS J1143+31	11:43:18.56	31:27:21.6	1.6	1793 ± 5	ID	UGC06684	11:43:20.70	31:27:20.9	1788	0.5	5				
-	-	-	-	-	-	UGC06684NOTES01	11:43:32.72	31:27:28.5	1813	3.0	20				
HIJASS J1144+48	11:44:23.71	48:49:40.4	1.9	899 ± 5	ID	UGC06713	11:44:24.97	48:50:06.8	899	0.5	0				
HIJASS J1145+50	11:45:06.26	50:18:02.4	3.4	1630 ± 15	ID	J114506.26+501802.4	11:45:06.26	50:18:02.4	1664	0.0	34				
HIJASS J1146+50	11:46:00.04	50:11:16.2	2.5	774 ± 11	ID	NGC3870	11:45:56.60	50:11:59.1	756	0.9	18				
HIJASS J1146+47	11:46:05.94	47:29:27.6	1.3	896 ± 5	ID	NGC3877	11:46:07.70	47:29:39.7	895	0.4	1				
-	-	-	-	-	-	J114605.86+472934.1	11:46:05.86	47:29:34.1	839	0.1	57				
HIJASS J1147+49	11:47:36.60	49:44:37.3	2.2	928 ± 7	ID	UGC06773	11:48:00.48	49:48:29.7	924	5.5	4				
HIJASS J1148+48	11:48:42.08	48:41:45.4	0.4	966 ± 3	ID	NGC3893	11:48:38.19	48:42:39.0	967	1.1	1				
-	-	-	-	-	-	NGC3896	11:48:56.39	48:40:28.8	905	2.7	61				
HIJASS J1149+39	11:49:25.09	39:45:48.1	2.2	849 ± 7	ID	UGC06792	11:49:23.28	39:46:16.6	841	0.6	8				
HIJASS J1149+48	11:49:39.66	48:25:11.1	1.1	962 ± 4	ID	NGC3906	11:49:40.50	48:25:33.5	961	0.4	1				
HIJASS J1149+51	11:49:56.16	51:51:01.3	3.0	1259 ± 11	ID	UGC06802	11:50:06.50	51:51:21.2	1256	1.6	3				
-	-	-	-	-	-	SBS1147+520	11:49:54.45	51:44:11.0	1257	6.8	2				
HIJASS J1150+45	11:50:43.51	45:47:54.9	2.0	811 ± 8	ID	UGC06818	11:50:46.95	45:48:25.9	808	0.8	3				
HIJASS J1150+51	11:50:43.95	51:48:45.4	1.1	960 ± 3	ID	NGC3917	11:50:45.43	51:49:28.8	965	0.8	5				
-	-	-	-	-	-	NGC3917A	11:51:13.45	52:00:03.1	837	12.2	123				
-	-	-	-	-	-	J115113.45+520003.1	11:51:13.45	52:00:03.1	908	12.2	52				
HIJASS J1150+38	11:50:51.08	38:52:25.5	0.2	242 ± 2	ID	UGC06817	11:50:52.99	38:52:49.0	242	0.5	0				
HIJASS J1151+38	11:51:44.54	38:01:06.2	0.7	915 ± 3	ID	NGC3930	11:51:46.01	38:00:54.4	919	0.4	4				
HIJASS J1151+48	11:51:48.05	48:40:27.2	1.5	983 ± 7	ID	NGC3928	11:51:47.62	48:40:59.3	988	0.5	5				
-	-	-	-	-	-	J115056.11+483153.8	11:50:56.11	48:31:53.8	968	12.1	15				
HIJASS J1152+52	11:52:05.80	52:06:00.5	1.2	1015 ± 4	ID	UGC06840	11:52:07.01	52:06:28.8	1046	0.5	31				
-	-	-	-	-	-	NGC3917A	11:51:13.45	52:00:03.1	837	10.0	178				
-	-	-	-	-	-	J115113.45+520003.1	11:51:13.45	52:00:03.1	908	10.0	107				
HIJASS J1152+44	11:52:47.46	44:06:56.1	0.4	808 ± 2	ID	NGC3938	11:52:49.45	44:07:14.6	809	0.5	1				
-	-	-	-	-	-	J115244.42+440602.0	11:52:44.42	44:06:02.0	842	1.1	34				
HIJASS J1152+50	11:52:48.60	50:00:18.7	1.7	994 ± 6	ID	UGC06849	11:52:39.16	50:02:16.0	995	2.5	1				
HIJASS J1152+37	11:52:53.66	37:00:19.9	1.5	934 ± 6	ID	NGC3941	11:52:55.36	36:59:10.8	928	1.2	6				
HIJASS J1153+47	11:53:37.84	47:51:14.4	1.8	790 ± 8	ID	NGC3949	11:53:41.72	47:51:31.4	800	0.7	10				
-	-	-	-	-	-	J115340.69+475156.4	11:53:40.70	47:51:56.5	855	0.8	65				
HIJASS J1153+52	11:53:44.96	52:18:35.9	0.9	1048 ± 4	ID	NGC3953	11:53:48.92	52:19:36.4	1052	1.2	4				
HIJASS J1154+30	11:54:12.17	30:07:20.9	1.9	974 ± 9	ID <sup>e</sup>	J115404.42+300634.6	11:54:04.42	30:06:34.6	981	1.8	7				

Table 2 – Continued

HJASS name (A1)	RA (J2000.0) (A2)	Dec. (J2000.0) (A3)	$\sigma_{\text{pos}}$ arcmin (A4)	$v_{\text{sys}} \pm \sigma_v$ km s <sup>-1</sup> (A5)	Class (A6)	NED ID <sup>a,b</sup> (A7)	RA (J2000.0) (A8)	Dec. (J2000.0) (A9)	vel. km s <sup>-1</sup> (A10)	pos. & vel. offsets arcmin (A11)	km s <sup>-1</sup> (A12)
HJASS J1156+50	11:56:24.96	50:25:04.9	0.6	915 ± 3	ID	UGC06917	11:56:26.52	50:25:43.2	911	0.7	4
HJASS J1156+48	11:56:36.58	48:19:30.9	0.9	945 ± 7	ID	NGC3985	11:56:42.11	48:20:02.2	948	1.1	3
HJASS J1157+50	11:57:02.98	50:48:51.5	1.1	894 ± 4	ID	UGC06922	11:56:52.15	50:49:01.2	877	1.7	17
HJASS J1157+49	11:57:16.03	49:16:24.7	0.7	776 ± 3	ID	UGC06930	11:57:17.35	49:16:59.1	777	0.6	1
HJASS J1157+53	11:57:32.85	53:20:51.6	1.0	1050 ± 4	ID	MESSIER109	11:57:35.98	53:22:28.3	1048	1.7	2
-	-	-	-	-	-	UGC06923	11:56:49.43	53:09:37.3	1066	13.0	16
-	-	-	-	-	-	UGC06940	11:57:47.58	53:14:04.1	1118	7.1	68
-	-	-	-	-	-	J115834.34+532043.8	11:58:34.34	53:20:43.8	1150	9.2	100
-	-	-	-	-	-	UGC06969	11:58:47.64	53:25:29.1	1114	12.1	64
-	-	-	-	-	-	J115649.85+530937.5	11:56:49.85	53:09:37.5	980	12.9	70
HJASS J1158+38	11:58:28.03	38:04:18.5	1.0	901 ± 4	ID	UGC06955	11:58:29.81	38:04:34.8	905	0.4	4
HJASS J1158+50	11:58:31.43	50:51:54.2	0.7	941 ± 5	ID	UGC06956	11:58:25.60	50:55:01.2	917	3.2	24
-	-	-	-	-	-	NGC4026	11:59:25.19	50:57:42.1	930	10.3	11
-	-	-	-	-	-	J115825.60+505501.2	11:58:25.60	50:55:01.2	839	3.2	102
HJASS J1158+43	11:58:33.83	43:56:27.3	1.2	829 ± 5	ID	NGC4013	11:58:31.38	43:56:47.7	831	0.6	2
HJASS J1158+47	11:58:37.08	47:14:47.4	1.4	904 ± 5	ID	NGC4010	11:58:37.89	47:15:41.4	902	0.9	2
HJASS J1158+42	11:58:44.97	42:43:06.7	1.6	713 ± 6	ID	IC0750	11:58:52.20	42:43:20.9	701	1.3	12
-	-	-	-	-	-	IC0749	11:58:34.05	42:44:02.5	807	2.2	94
-	-	-	-	-	-	J115851.31+424307.4	11:58:51.32	42:43:07.5	586	1.2	127
HJASS J1158+45	11:58:49.89	45:42:37.1	0.7	1148 ± 3	ID	UGCA259	11:58:53.27	45:44:04.1	1154	1.6	6
HJASS J1158+30	11:58:52.25	30:25:15.5	2.3	769 ± 8	ID	NGC4020	11:58:56.67	30:24:42.8	760	1.1	9
HJASS J1159+52	11:59:03.93	52:41:45.7	1.2	1084 ± 4	ID	UGC06983	11:59:09.28	52:42:27.0	1082	1.1	2
-	-	-	-	-	-	J115918.05+524234.2	11:59:18.05	52:42:34.3	1002	2.3	82
HJASS J1201+33	12:01:33.65	33:21:11.4	1.9	783 ± 8	ID	UGC07007	12:01:33.16	33:20:28.8	774	0.7	9
HJASS J1203+44	12:03:08.09	44:30:52.5	1.7	704 ± 8	ID	NGC4051	12:03:09.61	44:31:52.8	700	1.0	4
-	-	-	-	-	-	J120303.25+443225.4	12:03:03.25	44:32:25.4	770	1.8	66
HJASS J1204+52	12:04:00.36	52:34:51.9	0.2	205 ± 2	ID	NGC4068	12:04:00.78	52:35:17.8	210	0.4	5
HJASS J1204+31	12:04:03.75	31:54:05.6	2.5	759 ± 10	ID	NGC4062	12:04:03.83	31:53:44.9	758	0.3	1
HJASS J1205+50	12:05:31.72	50:30:56.1	0.6	753 ± 3	ID	NGC4088	12:05:34.19	50:32:20.5	757	1.5	4
-	-	-	-	-	-	NGC4085	12:05:22.71	50:21:10.6	746	9.9	7
-	-	-	-	-	-	J120543.59+503318.9	12:05:43.59	50:33:18.9	597	3.0	156
-	-	-	-	-	-	J120537.79+503304.6	12:05:37.79	50:33:04.6	645	2.3	108
-	-	-	-	-	-	J120531.00+503143.9	12:05:31.00	50:31:43.9	914	0.8	161
HJASS J1205+47	12:05:59.08	47:27:42.4	0.8	567 ± 6	ID	NGC4096	12:06:01.13	47:28:42.4	566	1.1	1
-	-	-	-	-	-	J120556.52+472625.9	12:05:56.52	47:26:25.9	381	1.3	186
HJASS J1206+49	12:06:07.98	49:34:30.6	1.1	1084 ± 9	ID	NGC4100	12:06:08.45	49:34:57.6	1074	0.5	10
-	-	-	-	-	-	J120608.59+493459.9	12:06:08.59	49:35:00.0	1097	0.5	13
HJASS J1206+43	12:06:25.27	43:03:15.8	2.1	805 ± 12	ID	NGC4111	12:07:03.13	43:03:56.6	807	6.9	2
-	-	-	-	-	-	UGC07089	12:05:57.74	43:08:36.0	770	7.3	35
-	-	-	-	-	-	J120559.63+425409.1	12:05:59.00	42:54:10.9	767	10.3	38

Table 2 – Continued

HIJASS name (A1)	RA		Dec. (J2000.0) (A3)	$\sigma_{\text{pos}}$ arcmin (A4)	$v_{\text{sys}} \pm \sigma_v$ km s <sup>-1</sup> (A5)	Class (A6)	NED ID <sup>a,b</sup> (A7)	RA		Dec. (J2000.0) (A9)	vel. km s <sup>-1</sup> (A10)	pos. & vel. offsets arcmin (A11)	km s <sup>-1</sup> (A12)
	(J2000.0) (A2)	(J2000.0) (A8)						(J2000.0) (A9)	(J2000.0) (A10)				
-	-	-	-	-	-	-	UGC07094	12:06:10.75	42:57:20.9	779	6.5	26	
-	-	-	-	-	-	-	NGC4117	12:07:46.11	43:07:34.9	934	15.4	129	
-	-	-	-	-	-	-	NGC4118	12:07:52.87	43:06:39.8	643	16.4	162	
HIJASS J1207+39	12:07:41.34	39:52:05.1	3.3	865 ± 8	ID	UGC4271	UGC4271	12:07:23.60	39:48:46.0	877	4.8	12	
HIJASS J1208+36	12:08:39.23	36:48:23.3	0.7	1070 ± 3	ID	UGC07125	UGC07125	12:08:42.33	36:48:09.9	1071	0.7	1	
HIJASS J1209+30	12:09:11.34	30:55:26.7	2.4	252 ± 9	ID	UGC07131	UGC07131	12:09:11.78	30:54:24.4	253	1.0	1	
HIJASS J1209+29	12:09:15.94	29:55:31.7	0.5	606 ± 3	ID	NGC4136	NGC4136	12:09:17.69	29:55:39.4	609	0.4	3	
HIJASS J1209+53	12:09:25.73	53:05:55.8	1.6	1163 ± 5	ID	NGC4142	NGC4142	12:09:30.19	53:06:17.8	1157	0.8	6	
HIJASS J1209+43A	12:09:29.34	43:40:02.5	1.5	893 ± 9	ID	NGC4138	NGC4138	12:09:29.78	43:41:07.1	888	1.1	5	
HIJASS J1209+43B	12:09:39.71	43:12:58.1	2.0	1057 ± 6	ID	UGC07146	UGC07146	12:09:49.15	43:14:04.9	1065	2.0	8	
HIJASS J1210+46	12:10:00.78	46:27:22.5	0.8	258 ± 3	ID	NGC4144	NGC4144	12:09:58.60	46:27:25.8	265	0.4	7	
HIJASS J1210+39A	12:10:03.97	39:52:17.4	0.4	1012 ± 2	ID	NGC4145	NGC4145	12:10:01.52	39:53:01.9	1009	0.9	3	
-	-	-	-	-	-	-	NGC4145A	12:10:54.54	39:45:26.5	1168	11.9	156	
HIJASS J1210+39B	12:10:32.06	39:23:52.3	0.3	997 ± 2	ID	NGC4151	NGC4151	12:10:32.58	39:24:20.6	995	0.5	2	
-	-	-	-	-	-	-	J121021.06+391252.1	12:10:21.07	39:12:52.2	919	11.2	78	
HIJASS J1211+50	12:11:02.67	50:28:17.1	0.7	776 ± 3	ID	NGC4157	NGC4157	12:11:04.37	50:29:04.8	774	0.8	2	
-	-	-	-	-	-	-	UGC07176	12:10:55.76	50:17:18.1	888	11.0	112	
-	-	-	-	-	-	-	MCG+08-22-082	12:11:22.57	50:16:10.3	899	12.5	123	
HIJASS J1212+36	12:12:07.87	36:10:17.5	0.5	164 ± 2	ID	NGC4163	NGC4163	12:12:09.16	36:10:09.1	165	0.3	1	
HIJASS J1212+29	12:12:20.62	29:12:07.5	0.9	1119 ± 4	ID	NGC4173	NGC4173	12:12:21.46	29:12:25.4	1127	0.3	8	
HIJASS J1212+37	12:12:21.44	37:00:16.3	1.8	1055 ± 7	ID	UGC07207	UGC07207	12:12:18.76	37:00:53.3	1051	0.8	4	
HIJASS J1213+52	12:13:02.25	52:17:04.4	2.3	778 ± 7	ID	UGC07218	UGC07218	12:12:56.52	52:15:55.3	770	1.4	8	
HIJASS J1213+43	12:13:13.93	43:41:41.7	0.9	929 ± 3	ID	NGC4183	NGC4183	12:13:16.88	43:41:54.9	930	0.6	1	
HIJASS J1213+24	12:13:45.66	24:15:20.9	1.3	948 ± 4	ID	UGC07236	UGC07236	12:13:49.15	24:15:53.2	945	1.0	3	
HIJASS J1213+36	12:13:47.85	36:37:22.4	0.3	229 ± 3	ID	NGC4190	NGC4190	12:13:44.77	36:38:02.5	228	0.9	1	
HIJASS J1215+35	12:15:01.40	35:56:56.6	1.5	939 ± 7	ID	UGC07257	UGC07257	12:15:02.96	35:57:30.6	942	0.6	3	
-	-	-	-	-	-	-	MCG+06-27-038	12:15:01.79	35:57:53.8	964	1.0	25	
HIJASS J1215+33	12:15:03.01	33:11:08.5	2.1	1089 ± 11	ID	NGC4203	NGC4203	12:15:05.05	33:11:50.4	1086	0.8	3	
-	-	-	-	-	-	-	J12153897+3309350 <sup>c</sup>	12:15:38.99	33:09:35.1	1067	7.7	22	
HIJASS J1215+51	12:15:19.81	51:21:11.8	1.2	462 ± 5	ID	UGC07267	UGC07267	12:15:23.65	51:20:59.6	472	0.6	10	
HIJASS J1215+43	12:15:33.62	43:24:40.0	1.2	555 ± 5	ID	UGC07271	UGC07271	12:15:33.44	43:26:02.8	547	1.4	8	
HIJASS J1215+36	12:15:36.48	36:19:35.4	0.1	291 ± 2	ID	NGC4214	NGC4214	12:15:39.17	36:19:36.8	291	0.5	0	
-	-	-	-	-	-	-	UGCA276	12:14:57.92	36:13:07.8	284	10.1	7	
-	-	-	-	-	-	-	HS1213+3636B	12:15:34.77	36:19:50.9	229	0.4	62	
HIJASS J1215+48	12:15:51.02	48:07:39.1	2.4	727 ± 8	ID	NGC4218	NGC4218	12:15:46.41	48:07:51.0	730	0.8	3	
-	-	-	-	-	-	-	J121546.41+480751.0	12:15:46.41	48:07:51.0	803	0.8	76	
HIJASS J1215+47	12:15:51.46	47:05:46.8	1.4	1031 ± 6	ID	NGC4217	NGC4217	12:15:50.90	47:05:30.4	1027	0.3	4	
HIJASS J1216+52	12:16:05.74	52:18:40.4	0.7	168 ± 3	ID	UGC07298	UGC07298	12:16:30.10	52:13:39.0	173	6.3	5	
-	-	-	-	-	-	-	CGCG269-049	12:15:46.62	52:23:13.9	159	5.4	9	
HIJASS J1216+46	12:16:42.36	46:03:53.2	2.0	707 ± 5	ID	UGC07301	UGC07301	12:16:42.08	46:04:43.6	690	0.8	17	

Table 2 – Continued

HJASS name (A1)	RA (J2000.0)		Dec. (J2000.0)	$\sigma_{\text{pos}}$ arcmin (A4)	$v_{\text{sys}} \pm \sigma_v$ km s <sup>-1</sup> (A5)	Class (A6)	NED ID <sup>a,b</sup> (A7)	RA (J2000.0)		Dec. (J2000.0)	vel. & vel. offsets	
	(A2)	(A3)						(A8)	(A9)		km s <sup>-1</sup> (A10)	arcmin (A11)
HJASS J1216+28	12:16:44.02	28:43:43.4	1.1	1210 ±4	ID	UGC07300	12:16:43.31	28:43:52.1	1210	0.2	0	
-	-	-	-	-	-	[YWP2010]J184.176+28.730	12:16:42.24	28:43:48.0	1218	0.4	8	
HJASS J1217+45	12:17:26.80	45:36:29.5	0.7	511 ±3	ID	NGC4242	12:17:30.18	45:37:09.5	506	0.9	5	
HJASS J1217+37	12:17:28.41	37:48:08.9	0.2	243 ±2	ID	NGC4244	12:17:29.66	37:48:25.6	244	0.4	1	
-	-	-	-	-	-	HS1214+3801	12:17:09.68	37:44:53.6	330	4.9	87	
HJASS J1217+22	12:17:34.22	22:32:42.3	1.5	400 ±6	ID	UGC07321	12:17:34.01	22:32:24.5	408	0.3	8	
HJASS J1218+46	12:18:11.04	46:55:01.2	1.8	333 ±5	ID	J121811.04+465501.2	12:18:11.07	46:55:00.7	472	0.0	139	
HJASS J1218+47	12:18:53.68	47:17:19.6	0.3	446 ±2	ID	MESSIER106	12:18:57.50	47:18:14.3	448	1.1	2	
-	-	-	-	-	-	NGC4248	12:17:49.85	47:24:33.1	484	13.0	38	
-	-	-	-	-	-	UGC07356	12:19:09.39	47:05:27.5	272	12.2	174	
-	-	-	-	-	-	J121855.34+471647.9	12:18:55.34	47:16:47.9	429	0.6	17	
-	-	-	-	-	-	J121901.36+471525.0	12:19:01.36	47:15:25.0	330	2.3	116	
HJASS J1219+46	12:19:52.78	46:35:27.3	1.2	392 ±3	PUO	-	-	-	-	-	-	
HJASS J1220+45	12:20:16.24	45:54:30.2	2.5	728 ±9	ID	UGC07391	12:20:16.24	45:54:30.2	612	0.0	116	
HJASS J1220+29	12:20:19.27	29:15:18.5	2.6	611 ±11	ID	NGC4278	12:20:06.82	29:16:50.7	649	3.1	38	
-	-	-	-	-	-	J122017.40+290609.1	12:20:17.40	29:06:09.1	710	9.2	99	
-	-	-	-	-	-	NGC4286	12:20:42.09	29:20:45.2	644	7.4	33	
HJASS J1220+47	12:20:34.85	47:49:04.8	2.4	729 ±9	ID	UGC07401	12:20:48.42	47:49:33.4	762	2.3	33	
HJASS J1220+46	12:20:36.67	46:17:14.0	0.5	518 ±5	ID	NGC4288	12:20:38.11	46:17:30.0	520	0.4	2	
HJASS J1220+38	12:20:56.87	38:25:06.9	1.2	574 ±4	ID	KUG1218+387	12:20:54.88	38:25:48.7	606	0.8	32	
HJASS J1221+45	12:21:14.29	45:48:02.6	0.3	460 ±2	ID	UGC07408	12:21:15.01	45:48:40.8	462	0.6	2	
-	-	-	-	-	-	UGC07391	12:20:16.24	45:54:30.2	612	12.0	152	
HJASS J1221+35	12:21:53.81	35:04:20.3	1.7	730 ±5	ID	UGC07427	12:21:54.86	35:03:00.3	724	1.4	6	
HJASS J1222+32	12:22:04.36	32:05:16.3	1.8	1144 ±7	ID	UGC07428	12:22:02.61	32:05:45.4	1137	0.6	7	
HJASS J1222+39	12:22:07.09	39:45:43.4	2.0	1073 ±5	ID	J122206.12+394452.4	12:22:06.12	39:44:52.4	1102	0.9	29	
HJASS J1224+31	12:24:11.84	31:30:47.1	3.4	1252 ±8	ID	NGC4359	12:24:11.17	31:31:19.0	1253	0.6	1	
HJASS J1224+39	12:24:33.18	39:21:47.2	2.7	1032 ±13	ID	NGC4369	12:24:36.20	39:22:58.8	1045	1.3	13	
HJASS J1225+26	12:25:22.45	26:43:48.7	2.8	318 ±12	ID	IC3308	12:25:18.21	26:42:54.4	316	1.3	2	
-	-	-	-	-	-	J122520.71+264210.2	12:25:20.71	26:42:10.2	342	1.7	24	
HJASS J1225+28	12:25:28.61	28:29:13.6	1.8	475 ±8	ID	O.321.0767130 <sup>f</sup>	12:25:29.15	28:28:56.8	483	0.3	8	
HJASS J1225+45	12:25:30.67	45:39:36.8	2.3	714 ±7	ID	NGC4389	12:25:35.10	45:41:04.8	718	1.7	4	
HJASS J1225+27	12:25:50.47	27:33:53.0	0.7	751 ±3	ID	NGC4393	12:25:51.23	27:33:41.6	755	0.3	4	
HJASS J1225+33	12:25:51.37	33:33:00.6	0.2	317 ±2	ID	NGC4395	12:25:48.86	33:32:48.9	319	0.6	2	
HJASS J1226+31	12:26:23.23	31:13:20.1	1.1	711 ±7	ID	NGC4414	12:26:27.10	31:13:24.7	716	0.8	5	
HJASS J1226+27	12:26:23.34	27:44:43.9	3.3	373 ±10	ID <sup>f</sup>	IC3341	12:26:23.19	27:44:43.9	372	0.0	1	
HJASS J1227+37	12:27:07.60	37:08:13.0	0.3	215 ±2	ID	UGC07559	12:27:05.15	37:08:33.4	218	0.6	3	
HJASS J1227+43	12:27:37.06	43:29:48.1	0.3	195 ±2	ID	UGC07577	12:27:40.90	43:29:44.0	195	0.7	0	
HJASS J1228+22A	12:28:02.83	22:35:15.8	1.7	592 ±4	ID	UGC07584	12:28:02.83	22:35:15.8	603	0.0	11	
HJASS J1228+44	12:28:06.33	44:05:56.9	0.1	205 ±3	ID	NGC4449	12:28:11.10	44:05:37.1	207	0.9	2	
HJASS J1228+37	12:28:21.72	37:13:53.7	0.5	260 ±4	ID	UGC07599	12:28:28.56	37:14:01.1	278	1.4	18	

Table 2 – Continued

HIJASS name (A1)	RA (J2000.0)		Dec. (J2000.0)	$\sigma_{\text{pos}}$ arcmin (A4)	$v_{\text{sys}} \pm \sigma_v$ km s <sup>-1</sup> (A5)	Class (A6)	NED ID <sup>a,b</sup> (A7)	RA (J2000.0)		Dec. (J2000.0)	vel. km s <sup>-1</sup> (A10)	pos. & vel. offsets arcmin (A11) km s <sup>-1</sup> (A12)	
	(A2)	(A3)						(A8)	(A9)			(A11)	(A12)
HIJASS J1228+35	12:28:36.15	35:43:36.4	1.2	311 ± 5	ID	UGC07605	12:28:38.74	35:43:02.9	310	0.8	1		
HIJASS J1228+43	12:28:41.00	43:13:13.9	0.3	536 ± 2	ID	UGC07608	12:28:44.20	43:13:26.9	538	0.6	2		
HIJASS J1228+22B	12:28:41.92	22:49:00.3	0.6	642 ± 2	ID	NGC4455	12:28:44.11	22:49:13.6	637	0.6	5		
HIJASS J1228+42	12:28:52.22	42:10:40.5	2.0	417 ± 9	ID	MCG+07-26-011	12:28:52.23	42:10:40.5	408	0.0	9		
HIJASS J1230+42	12:30:23.57	42:54:05.7	1.5	381 ± 7	ID	MCG+07-26-012	12:30:23.57	42:54:05.7	436	0.0	55		
HIJASS J1230+41	12:30:32.63	41:38:33.7	0.2	570 ± 4	ID	J123023.60+425405.7 NGC4490	12:30:36.24	41:38:38.0	522	0.0	141		
HIJASS J1231+29	12:31:56.48	29:42:25.7	1.6	644 ± 4	ID	UGC07673	12:30:31.13	41:42:04.2	565	0.7	5		
HIJASS J1232+39	12:32:04.84	39:48:18.7	0.9	680 ± 4	ID	UGC07678	12:31:58.57	29:42:34.6	493	3.5	77		
HIJASS J1232+42	12:32:26.69	42:41:41.1	1.0	538 ± 4	ID	UGC07690	12:32:00.17	39:49:57.6	642	0.5	2		
HIJASS J1232+37	12:32:46.41	37:37:45.9	1.4	503 ± 6	ID	UGC07699	12:32:26.89	42:42:14.8	666	1.9	14		
HIJASS J1232+31	12:32:53.44	31:32:48.6	0.5	331 ± 2	ID	UGC07698	12:32:48.02	37:37:18.4	537	0.6	1		
HIJASS J1233+32	12:33:04.71	32:06:54.2	2.1	923 ± 9	ID	NGC4509	12:32:54.39	31:32:28.0	496	0.6	7		
HIJASS J1233+33	12:33:15.73	33:20:19.4	2.3	830 ± 12	ID	J123306.44+320527.4	12:33:06.44	32:05:29.7	937	1.5	14		
HIJASS J1233+24 <sup>f</sup>	12:33:39.50	23:59:07.8	3.3	1316 ± 16	ID <sup>f</sup>	KUG1230+336	12:33:24.89	33:21:04.5	912	1.5	11		
HIJASS J1233+39	12:33:48.83	39:38:43.4	1.2	658 ± 4	ID	O.378.0206985 <sup>f</sup>	12:33:41.75	23:59:13.6	838	2.1	8		
HIJASS J1233+30	12:33:55.58	30:17:56.4	2.3	1173 ± 11	ID	MCG+07-26-024	12:33:52.74	39:37:33.4	1325	0.5	9		
HIJASS J1234+39	12:34:03.47	39:00:39.9	1.4	679 ± 4	ID	NGC4525	12:33:51.14	30:16:38.9	646	1.4	12		
HIJASS J1234+35	12:34:04.03	35:31:37.7	0.4	802 ± 2	ID	UGC07719	12:34:00.54	39:01:09.0	1172	1.6	1		
HIJASS J1235+41	12:35:13.31	41:03:07.7	2.0	608 ± 6	ID	NGC4534	12:34:05.42	35:31:06.0	678	0.7	1		
HIJASS J1235+27	12:35:57.46	27:57:32.3	0.2	813 ± 2	ID	UGC07751	12:35:11.77	41:03:39.5	802	0.6	0		
HIJASS J1236+25	12:36:16.77	25:59:43.3	0.3	1226 ± 3	ID	NGC4559	12:35:57.65	27:57:36.0	605	0.6	3		
HIJASS J1236+40	12:36:19.65	40:00:01.1	1.5	522 ± 5	ID	J123551.86+275557.0	12:35:51.86	27:55:57.0	807	0.1	6		
HIJASS J1238+32	12:38:37.28	32:45:53.4	0.4	309 ± 2	ID	NGC4565	12:36:20.78	25:59:15.6	855	2.0	42		
HIJASS J1239+44	12:39:44.52	44:49:11.1	1.3	554 ± 4	ID	NGC4562	12:36:20.78	25:59:15.6	1230	1.0	4		
HIJASS J1240+32	12:40:10.00	32:39:30.0	1.2	759 ± 6	ID	IC3571	12:35:34.80	25:51:00.0	1353	12.8	127		
HIJASS J1241+41	12:41:38.22	41:11:02.9	0.4	556 ± 3	ID	UGC07774	12:36:20.10	26:05:03.2	1260	5.4	34		
HIJASS J1242+32	12:42:06.94	32:31:54.0	0.1	610 ± 2	ID	UGC07774	12:36:22.72	40:00:18.7	526	0.7	4		
HIJASS J1242+38	12:42:15.55	38:30:38.5	0.7	354 ± 3	ID	UGCA292	12:38:40.06	32:46:00.5	308	0.6	1		
HIJASS J1243+24	12:43:05.87	24:27:03.9	2.8	1823 ± 6	ID <sup>f</sup>	UGC07827	12:39:38.93	44:49:14.4	554	1.0	0		
HIJASS J1243+32	12:43:51.42	32:10:18.4	0.1	642 ± 3	ID	J124010.08+323930.4	12:40:10.04	32:39:31.6	776	0.0	17		
-	-	-	-	-	-	NGC4618	12:41:32.85	41:09:02.8	544	2.2	12		
-	-	-	-	-	-	NGC4625	12:41:52.72	41:16:26.3	598	6.0	42		
-	-	-	-	-	-	NGC4631	12:42:08.01	32:32:29.4	606	0.6	4		
-	-	-	-	-	-	J124146.99+325124.8	12:41:47.13	32:51:24.9	696	20.0	86		
-	-	-	-	-	-	NGC4627	12:41:59.68	32:34:24.8	542	2.9	68		
HIJASS J1242+38	12:42:15.55	38:30:38.5	0.7	354 ± 3	ID	IC3687	12:42:15.10	38:30:12.0	354	0.5	0		
HIJASS J1243+24	12:43:05.87	24:27:03.9	2.8	1823 ± 6	ID <sup>f</sup>	KUG1240+247	12:43:05.87	24:27:03.9	1825	0.0	2		
HIJASS J1243+32	12:43:51.42	32:10:18.4	0.1	642 ± 3	ID	NGC4656NED01	12:43:57.67	32:10:12.9	664	1.3	22		
-	-	-	-	-	-	J124348.72+320813.8	12:43:48.72	32:08:13.8	705	2.2	63		

Table 2 – Continued

HIIASS name (A1)	RA (J2000.0) (A2)	Dec. (J2000.0) (A3)	$\sigma_{\text{pos}}$ arcmin (A4)	$v_{\text{sys}} \pm \sigma_v$ km s <sup>-1</sup> (A5)	Class (A6)	NED ID <sup>a,b</sup> (A7)	RA (J2000.0) (A8)	Dec. (J2000.0) (A9)	vel. km s <sup>-1</sup> (A10)	pos. & vel. offsets arcmin (A11)	km s <sup>-1</sup> (A12)
-	-	-	-	-	-	J12440599+3212340 <sup>c</sup>	12:44:05.98	32:12:32.3	617	3.8	25
HIIASS J1244+34	12:44:25.63	34:23:24.7	0.7	601 ± 2	ID	UGC07916	12:44:25.14	34:23:11.5	607	0.2	6
HIIASS J1244+28	12:44:36.09	28:28:46.4	1.9	936 ± 6	ID	UGCA294	12:44:38.15	28:28:21.0	947	0.6	11
HIIASS J1245+27	12:45:16.60	27:07:02.9	1.9	1077 ± 10	ID	NGC4670	12:45:17.07	27:07:31.5	1069	0.5	8
-	-	-	-	-	-	J124516.87+270730.7	12:45:16.87	27:07:30.8	1045	0.5	32
HIIASS J1246+36	12:46:58.34	36:28:33.1	0.7	332 ± 3	ID	UGC07949	12:46:59.80	36:28:35.0	331	0.3	1
HIIASS J1250+25	12:50:23.64	25:30:27.1	0.2	1205 ± 3	ID	NGC4725	12:50:26.58	25:30:02.9	1206	0.8	1
HIIASS J1250+41	12:50:54.65	41:06:50.3	0.8	304 ± 4	ID	MESSIER094	12:50:53.06	41:07:13.7	308	0.5	4
HIIASS J1251+26	12:51:44.44	26:06:37.8	1.5	1241 ± 7	ID	KUG1249+263	12:51:44.45	26:06:37.8	1225	0.0	16
HIIASS J1251+25	12:51:47.91	25:48:27.3	0.3	1201 ± 5	ID	NGC4747	12:51:45.95	25:46:37.5	1190	1.9	11
HIIASS J1254+27	12:54:03.66	27:09:27.1	0.3	373 ± 2	ID	NGC4789A	12:54:05.25	27:08:58.7	374	0.6	1

<sup>a</sup> The most likely counterpart of a HIIASS source is given in the first row. Potentially confused HIIASS sources, with multiple galaxies within the gridded beam or the H I intensity contours (for large sources) and within the velocity range of the H I detection, are listed in the subsequent rows.

<sup>b</sup> Unless stated differently, identifications starting with 'J' are SDSS galaxies and their full names are of the form: SDSS X, where X is the stated ID.

<sup>c</sup> 2MASX objects with full identifications of the form: 2MASX Y, where Y is the stated ID.

<sup>d</sup> MAPS-NGP object with full identification of the form: MAPS-NGP Z, where Z is the stated ID.

<sup>e</sup> Redshift information available in SDSS DR8 (Aihara et al. 2011) – not listed in NED.

<sup>f</sup> Redshift information available in ALFALFA (Haynes et al. 2011) – not listed in NED.

<sup>g</sup> HIIASS name consistent with Lang et al. (2003).

Table 3: The HI properties of all HIJASS detections

HIJASS name (B1)	$S_p$		$S_p(\text{corr})$		$\sigma_{\text{peak}}$		$S_{\text{int}}$		$S_{\text{int}}(\text{corr})$		$\sigma_{\text{int}}$		$W_{50} \pm \sigma_{50}$		$W_{20} \pm \sigma_{20}$		rms		Distance		flags <sup>a</sup> (B13)
	Jy (B2)	Jy (B3)	Jy (B4)	Jy km s <sup>-1</sup> (B5)	Jy km s <sup>-1</sup> (B6)	Jy km s <sup>-1</sup> (B7)	km s <sup>-1</sup> (B8)	km s <sup>-1</sup> (B9)	Jy (B10)	Mpc (B11)	$\log M_{\text{HI}}$ (B12)										
HIJASS J1048+46	0.059	-	0.012	4.22	-	1.73	98±12	110±18	0.012	11.1	8.09										
HIJASS J1054+49	0.101	0.091	0.021	10.35	11.54	3.83	124±30	173±45	0.020	20.0	9.04										
HIJASS J1102+52	0.106	-	0.017	4.39	-	1.75	46±14	68±21	0.016	14.5	8.34										
HIJASS J1108+53	0.109	0.098	0.017	8.75	9.76	2.72	94±12	109±18	0.016	18.6	8.50										
HIJASS J1109+50	0.074	-	0.010	6.91	-	1.48	125±12	155±21	0.009	13.9	8.90										
HIJASS J1110+46	0.069	-	0.011	6.54	-	1.66	120±12	135±18	0.010	20.7	8.82										
HIJASS J1113+53	0.269	-	0.017	10.76	-	1.08	44±4	61±6	0.010	14.4	8.72										
HIJASS J1120+53	0.560	-	0.031	49.6	-	2.08	101±4	125±6	0.013	17.1	9.53										
HIJASS J1123+50	0.069	-	0.014	8.48	-	2.64	177±14	193±21	0.014	17.1	8.77										
HIJASS J1123+52	0.218	-	0.015	34.23	-	2.13	197±6	219±9	0.010	18.4	9.44										
HIJASS J1126+53	0.333	0.298	0.027	35.95	40.3	4.35	130±6	142±9	0.022	10.4	9.01										
HIJASS J1132+53	0.540	0.477	0.032	151.09	170.97	6.77	467±6	488±9	0.021	17.1	10.07										
HIJASS J1132+39	0.103	-	0.014	8.11	-	1.96	82±14	115±21	0.013	22.5	8.98										
HIJASS J1133+47	0.532	0.476	0.033	94.21	105.75	5.83	262±6	282±9	0.023	17.1	9.86										
HIJASS J1133+49	0.059	-	0.009	2.12	-	0.92	40±10	52±15	0.009	4.2	6.95										
HIJASS J1136+45	0.622	-	0.033	48.51	-	1.50	83±4	100±6	0.010	3.2	8.07										
HIJASS J1136+36	0.174	0.157	0.019	40.68	45.41	4.92	267±10	289±15	0.017	22.5	9.73										
HIJASS J1137+47	0.354	0.317	0.022	53.33	59.8	3.51	213±8	255±12	0.015	17.1	9.61										
HIJASS J1138+35	0.104	0.097	0.014	10.38	11.35	2.39	160±16	197±24	0.013	23.2	9.16										
HIJASS J1138+33	0.078	0.072	0.013	9.81	10.82	2.50	199±12	212±18	0.012	26.3	9.25										
HIJASS J1138+43	0.047	-	0.006	5.26	-	1.08	156±16	206±24	0.006	17.1	8.56										
HIJASS J1139+46	0.346	-	0.022	28.55	-	2.01	89±6	125±9	0.013	17.1	9.29										
HIJASS J1140+45	0.655	0.587	0.037	25.7	28.8	2.62	41±4	59±6	0.022	17.1	9.30										
HIJASS J1141+46	0.057	-	0.008	4.45	-	1.05	103±10	121±15	0.007	17.1	8.49										
HIJASS J1141+36	0.147	0.134	0.017	32.24	35.73	4.45	273±14	312±21	0.016	21.0	9.57										
HIJASS J1141+32	0.093	0.085	0.014	9.60	10.62	2.47	129±16	158±24	0.013	25.8	9.22										
HIJASS J1142+51	0.058	-	0.010	8.75	-	2.09	184±20	225±30	0.010	17.1	8.78										
HIJASS J1143+31	0.064	-	0.009	7.62	-	1.49	148±10	165±15	0.008	25.4	9.06										
HIJASS J1144+48	0.176	0.159	0.024	13.09	14.61	3.75	88±10	104±15	0.023	17.1	9.00										
HIJASS J1145+50	0.042	-	0.011	2.48	-	1.44	71±30	109±45	0.011	24.3	8.54										
HIJASS J1146+50	0.068	-	0.013	5.18	-	1.93	86±22	129±33	0.013	17.1	8.55										
HIJASS J1146+47	0.099	-	0.011	18.65	-	2.34	337±10	363±15	0.010	17.1	9.11										
HIJASS J1147+49	0.070	-	0.013	2.74	-	1.28	75±14	93±21	0.012	17.1	8.28										
HIJASS J1148+48	0.348	-	0.020	82.6	-	2.62	262±6	306±9	0.010	17.1	9.76										
HIJASS J1149+39	0.123	0.114	0.020	12.05	13.25	3.49	158±14	175±21	0.019	12.5	8.69										
HIJASS J1149+48	0.137	-	0.014	5.39	-	1.28	42±8	58±12	0.012	17.1	8.57										
HIJASS J1149+51	0.052	-	0.012	5.75	-	2.15	152±22	178±33	0.012	19.1	8.70										
HIJASS J1150+45	0.100	0.093	0.015	11.74	12.91	2.81	146±16	173±24	0.014	17.1	8.95										

Table 3 – Continued

HIJASS name (B1)	$S_p$		$S_p(\text{corr})$		$\sigma_{\text{peak}}$		$S_{\text{int}}$		$S_{\text{int}}(\text{corr})$		$\sigma_{\text{int}}$		$W_{50} \pm \sigma_{50}$		$W_{20} \pm \sigma_{20}$		rms		Distance		$\log M_{\text{HI}}$		flags <sup>a</sup> (B13)
	Jy	(B2)	Jy	(B3)	Jy	(B4)	Jy	(B5)	Jy	(B6)	Jy	(B7)	km s <sup>-1</sup>	(B8)	km s <sup>-1</sup>	(B9)	Jy	(B10)	Mpc	(B11)	(B12)	(B13)	
HIJASS J1150+51	0.130	-	-	-	23.81	-	-	2.53	-	-	-	2.53	278±6	292±9	0.011	17.1	9.21	cd					
HIJASS J1150+38	0.926	-	-	-	38.26	-	-	1.31	-	-	-	1.31	42±4	68±6	0.012	2.6	7.80	vi					
HIJASS J1151+38	0.235	0.210	-	-	28.21	31.66	-	2.51	-	-	-	2.51	151±6	168±9	0.012	13.3	9.12	e3					
HIJASS J1151+48	0.090	-	-	-	6.06	-	-	1.40	-	-	-	1.40	63±14	102±21	0.010	16.9	8.61	ci					
HIJASS J1152+52	0.116	-	-	-	14.28	-	-	2.08	-	-	-	2.08	138±8	158±12	0.011	17.1	8.99	cd					
HIJASS J1152+44	0.904	0.808	-	-	76.02	85.37	-	4.02	-	-	-	4.02	93±4	112±6	0.023	17.1	9.77	ec					
HIJASS J1152+50	0.076	-	-	-	5.61	-	-	1.46	-	-	-	1.46	88±12	108±18	0.010	17.1	8.59	i					
HIJASS J1152+37	0.078	-	-	-	15.29	-	-	2.14	-	-	-	2.14	262±12	286±18	0.009	12.2	8.73	i					
HIJASS J1153+47	0.207	0.187	-	-	41.31	46.01	-	6.94	-	-	-	6.94	251±16	282±24	0.026	17.1	9.50	ec					
HIJASS J1153+52	0.165	-	-	-	38.2	-	-	2.85	-	-	-	2.85	403±8	427±12	0.011	17.1	9.42	d					
HIJASS J1154+30	0.063	-	-	-	3.58	-	-	1.15	-	-	-	1.15	51±18	91±27	0.009	13.6	8.20	n					
HIJASS J1156+50	0.164	-	-	-	22.83	-	-	1.61	-	-	-	1.61	184±6	206±9	0.008	17.1	9.20	d5					
HIJASS J1156+48	0.140	-	-	-	13.21	-	-	1.65	-	-	-	1.65	92±14	169±21	0.010	17.1	8.96	d					
HIJASS J1157+50	0.107	-	-	-	8.93	-	-	1.40	-	-	-	1.40	118±8	139±12	0.009	17.1	8.79	d					
HIJASS J1157+49	0.359	0.323	0.023	-	37.53	41.95	-	3.30	-	-	-	3.30	121±6	138±9	0.017	17.1	9.46	e					
HIJASS J1157+53	0.306	0.271	0.025	-	80.95	91.39	-	6.56	-	-	-	6.56	457±8	484±12	0.021	17.1	9.80	ec					
HIJASS J1158+38	0.297	0.266	0.025	-	35.33	39.61	-	4.36	-	-	-	4.36	148±8	166±12	0.021	13.2	9.21	e					
HIJASS J1158+50	0.207	-	-	-	11.46	-	-	1.39	-	-	-	1.39	58±10	120±15	0.011	17.1	8.90	cd					
HIJASS J1158+43	0.189	0.174	0.018	-	34.32	37.86	-	4.02	-	-	-	4.02	387±10	411±15	0.016	17.1	9.42	e					
HIJASS J1158+47	0.161	0.146	0.018	-	34.19	38.03	-	4.39	-	-	-	4.39	253±10	275±15	0.016	17.1	9.42	e					
HIJASS J1158+42	0.103	0.097	0.013	-	22.2	24.21	-	3.23	-	-	-	3.23	366±12	389±18	0.012	17.1	9.22	ec					
HIJASS J1158+45	0.142	-	-	-	6.43	-	-	0.92	-	-	-	0.92	46±6	62±9	0.008	17.1	8.65	e					
HIJASS J1158+30	0.099	0.091	0.017	-	12.35	13.63	-	3.33	-	-	-	3.33	152±16	172±24	0.016	10.8	8.57	e					
HIJASS J1159+52	0.242	0.218	0.023	-	30.03	33.52	-	4.22	-	-	-	4.22	175±8	191±12	0.020	17.1	9.36	ec					
HIJASS J1201+33	0.070	-	-	-	2.86	-	-	1.09	-	-	-	1.09	51±16	82±24	0.010	11.2	7.93	ec					
HIJASS J1203+44	0.185	0.168	0.024	-	34.28	38.08	-	5.64	-	-	-	5.64	237±16	278±24	0.022	17.1	9.42	ec					
HIJASS J1204+52	0.623	-	-	-	32.31	-	-	1.23	-	-	-	1.23	55±4	81±6	0.010	4.4	8.16	vi					
HIJASS J1204+31	0.110	0.103	0.021	-	20.58	22.5	-	5.03	-	-	-	5.03	295±20	327±30	0.020	10.8	8.79	e					
HIJASS J1205+50	0.529	0.463	0.032	-	137.08	156.12	-	6.87	-	-	-	6.87	330±6	354±9	0.022	17.1	10.03	ec					
HIJASS J1205+47	0.420	0.378	0.030	-	72.0	80.54	-	5.71	-	-	-	5.71	250±12	327±18	0.023	9.1	9.19	ec					
HIJASS J1206+49	0.219	0.199	0.020	-	37.93	42.17	-	4.21	-	-	-	4.21	282±18	376±27	0.017	17.1	9.46	ec					
HIJASS J1206+43	0.284	0.231	0.039	-	47.59	59.63	-	10.12	-	-	-	10.12	230±24	287±36	0.037	15.0	9.50	eci					
HIJASS J1207+39	0.092	0.080	0.020	-	2.49	2.86	-	2.04	-	-	-	2.04	48±16	62±24	0.020	12.8	8.05	e					
HIJASS J1208+36	0.442	0.391	0.029	-	50.16	56.75	-	4.31	-	-	-	4.31	149±6	166±9	0.021	15.6	9.51	e					
HIJASS J1209+30	0.065	-	-	-	6.58	-	-	2.05	-	-	-	2.05	115±18	142±27	0.012	3.5	7.28	v					
HIJASS J1209+29	0.596	0.529	0.034	-	51.36	57.95	-	3.92	-	-	-	3.92	88±6	110±9	0.022	8.5	8.99	e					
HIJASS J1209+53	0.081	-	-	-	11.46	-	-	2.02	-	-	-	2.02	173±10	188±15	0.010	17.1	8.90	e					
HIJASS J1209+43A	0.093	-	-	-	20.08	-	-	2.75	-	-	-	2.75	277±18	336±27	0.011	13.8	8.95	i					
HIJASS J1209+43B	0.065	-	-	-	3.79	-	-	1.30	-	-	-	1.30	67±12	82±18	0.010	17.1	8.42	n					
HIJASS J1210+46	0.429	0.384	0.031	-	57.29	64.28	-	5.28	-	-	-	5.28	160±6	181±9	0.024	6.9	8.85	evi					



Table 3 – Continued

HIJASS name (B1)	$S_p$		$S_p(\text{corr})$		$\sigma_{\text{peak}}$	$S_{\text{int}}$		$S_{\text{int}}(\text{corr})$		$\sigma_{\text{int}}$	$w_{50} \pm \sigma_{50}$	$w_{20} \pm \sigma_{20}$	rms	Distance	$\log M_{\text{HI}}$	flags <sup>a</sup> (B13)				
	Jy	(B2)	Jy	(B3)	Jy	(B4)	Jy km s <sup>-1</sup>	(B5)	Jy km s <sup>-1</sup>	(B6)	Jy km s <sup>-1</sup>	(B7)	km s <sup>-1</sup>	(B8)	km s <sup>-1</sup>		(B9)	Jy	(B10)	Mpc
HIJASS J1210+39A	0.361	-	-	-	0.021	57.04	-	2.35	-	218±4	235±6	0.011	15.0	9.48	cd					
HIJASS J1210+39B	0.559	-	-	-	0.030	51.97	-	1.97	-	121±4	141±6	0.012	14.7	9.42	cd					
HIJASS J1211+50	0.489	0.436	0.033	137.23	0.014	122.01	137.23	7.55	398±6	422±9	0.025	17.1	9.98	ec						
HIJASS J1212+36	0.226	-	0.014	6.96	0.031	43.48	48.65	5.01	159±8	179±12	0.025	15.8	9.46	e						
HIJASS J1212+29	0.391	-	0.014	6.89	0.010	4.03	-	1.88	79±14	106±21	0.013	15.4	8.58							
HIJASS J1212+37	0.095	-	0.010	4.03	0.030	57.46	64.38	5.88	86±14	105±21	0.010	17.1	8.44							
HIJASS J1213+52	0.056	-	0.009	3.97	0.024	20.02	-	0.96	235±6	252±9	0.025	17.1	9.65	e						
HIJASS J1213+43	0.376	-	0.009	3.97	0.018	12.1	13.57	2.65	56±8	71±12	0.008	13.0	8.20							
HIJASS J1213+24	0.080	-	0.024	20.02	0.013	7.64	-	2.29	51±6	76±9	0.011	2.8	7.57	dbvi						
HIJASS J1213+36	0.424	-	0.014	6.89	0.018	12.1	13.57	2.65	75±14	111±21	0.016	13.7	8.78	ec						
HIJASS J1215+35	0.160	0.143	0.018	12.1	0.024	30.21	33.76	5.95	232±22	291±33	0.023	15.1	9.26	eci						
HIJASS J1215+33	0.162	0.146	0.024	30.21	0.011	11.14	-	1.74	114±10	147±15	0.010	7.9	8.21							
HIJASS J1215+51	0.106	-	0.011	11.14	0.008	5.82	-	1.03	89±10	115±15	0.007	8.7	8.01							
HIJASS J1215+43	0.078	-	0.172	206.03	0.013	7.64	-	2.29	64±4	90±6	0.011	2.9	8.60	cdbvi						
HIJASS J1215+36	3.438	-	0.013	7.64	0.014	34.83	-	3.72	140±16	165±24	0.013	17.1	8.72	c						
HIJASS J1215+48	0.071	-	0.014	34.83	0.019	8.68	10.13	1.52	390±12	421±18	0.013	17.1	9.38	5						
HIJASS J1215+47	0.123	-	0.014	34.83	0.008	5.98	-	1.45	34±6	55±9	0.014	4.2	7.62	eevi						
HIJASS J1216+52	0.293	0.250	0.019	8.68	0.008	5.98	-	1.45	143±10	155±15	0.008	17.1	8.61							
HIJASS J1216+46	0.053	-	0.008	5.98	0.016	11.7	13.01	2.08	69±8	94±12	0.014	17.1	8.95	e						
HIJASS J1216+28	0.189	0.171	0.016	11.7	0.029	42.27	47.27	4.16	114±6	135±9	0.022	8.2	8.88	e						
HIJASS J1217+45	0.426	0.383	0.029	42.27	0.117	377.52	437.73	6.63	201±4	221±6	0.028	4.3	9.28	ecbvi						
HIJASS J1217+37	2.639	2.263	0.117	377.52	0.028	35.4	39.42	5.88	221±12	252±18	0.026	5.1	8.39	e						
HIJASS J1217+22	0.246	0.223	0.028	35.4	0.012	6.26	-	1.67	164±10	177±15	0.011	5.8	7.69	fdnb						
HIJASS J1218+46	0.079	-	0.012	6.26	0.068	457.69	540.16	9.97	417±4	440±6	0.028	7.6	9.87	ecdi						
HIJASS J1218+47	1.463	1.233	0.068	457.69	0.008	2.36	-	0.66	34±6	47±9	0.007	6.6	7.38	dn						
HIJASS J1219+46	0.076	-	0.008	2.36	0.009	3.21	-	1.25	79±18	110±27	0.009	17.1	8.34	f						
HIJASS J1220+45	0.048	-	0.009	3.21	0.009	10.47	-	2.31	392±22	432±33	0.009	16.1	8.81	ci						
HIJASS J1220+29	0.046	-	0.009	10.47	0.013	3.13	-	1.47	49±18	80±27	0.013	17.1	8.33	3						
HIJASS J1220+47	0.071	-	0.013	3.13	0.015	36.51	-	1.93	173±10	243±15	0.009	8.4	8.78	d						
HIJASS J1220+46	0.229	-	0.015	36.51	0.013	3.51	-	0.99	31±8	53±12	0.011	8.7	7.79							
HIJASS J1220+38	0.125	-	0.013	3.51	0.014	8.51	-	0.60	32±4	53±6	0.006	7.5	8.05	dc						
HIJASS J1221+45	0.248	-	0.014	8.51	0.011	3.29	-	1.11	46±10	60±15	0.010	10.7	7.95							
HIJASS J1221+35	0.077	-	0.011	3.29	0.019	8.67	9.63	2.61	61±14	89±21	0.018	16.4	8.79	e						
HIJASS J1222+32	0.146	0.133	0.019	8.67	0.011	2.90	-	1.13	52±10	64±15	0.010	15.9	8.24	n						
HIJASS J1222+39	0.066	-	0.011	2.90	0.034	20.06	22.32	7.44	195±16	207±24	0.033	17.9	9.23	e						
HIJASS J1224+31	0.140	0.127	0.034	20.06	0.012	5.72	-	2.01	107±26	158±39	0.012	15.3	8.50							
HIJASS J1224+39	0.059	-	0.012	5.72	0.024	14.36	15.82	4.76	137±24	172±36	0.023	5.1	7.98	eci						
HIJASS J1225+26	0.116	0.107	0.024	14.36	0.020	6.84	7.66	2.43	44±16	81±24	0.019	6.6	7.90	e						
HIJASS J1225+28	0.151	0.136	0.020	6.84	0.009	7.14	-	1.79	168±14	189±21	0.009	17.1	8.69							
HIJASS J1225+45	0.052	-	0.009	7.14																

Table 3 – Continued

HIJASS name (B1)	$S_p$		$S_p(\text{corr})$		$\sigma_{\text{peak}}$	$S_{\text{int}}$		$S_{\text{int}}(\text{corr})$		$\sigma_{\text{int}}$	$W_{50} \pm \sigma_{50}$		$W_{20} \pm \sigma_{20}$		rms	Distance	$\log M_{\text{HI}}$	flags <sup>a</sup> (B13)
	Jy	(B2)	Jy	(B3)	Jy	Jy km s <sup>-1</sup>	(B5)	Jy km s <sup>-1</sup>	(B6)	Jy km s <sup>-1</sup>	(B7)	km s <sup>-1</sup>	(B8)	km s <sup>-1</sup>	(B9)	Jy	(B10)	
HIJASS J1225+27	0.434	0.389	0.029	0.029	44.84	50.27	4.26	122±6	145±9	0.022	10.5	9.12	e					
HIJASS J1225+33	3.067	2.681	0.139	0.139	315.03	359.38	7.29	118±4	138±6	0.037	4.7	9.28	ei					
HIJASS J1226+31	0.310	0.278	0.028	0.028	74.1	83.04	7.06	354±14	421±21	0.024	17.7	9.79	ei					
HIJASS J1226+27	0.040	-	0.010	-	2.40	-	1.32	73±20	92±30	0.010	5.2	7.18	f					
HIJASS J1227+37	0.407	-	0.023	-	24.78	-	1.33	64±4	87±6	0.010	5.0	8.16	dvi					
HIJASS J1227+43	0.546	-	0.030	-	13.88	-	1.12	28±4	42±6	0.013	2.6	7.34	dbvi					
HIJASS J1228+22A	0.069	-	0.010	-	3.14	-	1.03	49±8	59±12	0.009	8.0	7.67	df					
HIJASS J1228+44	2.752	-	0.138	-	250.36	-	2.43	91±6	142±9	0.015	4.3	9.03	dvi					
HIJASS J1228+37	0.180	-	0.011	-	12.03	-	0.97	69±8	110±12	0.007	4.7	7.80	dvi					
HIJASS J1228+35	0.191	0.173	0.018	0.018	5.20	5.79	1.58	29±10	55±15	0.016	4.7	7.49	e5i					
HIJASS J1228+43	0.498	-	0.027	-	26.04	-	1.35	59±4	76±6	0.011	8.5	8.65	b					
HIJASS J1228+22B	0.243	-	0.016	-	30.18	-	2.09	136±4	153±6	0.011	8.7	8.73	d					
HIJASS J1228+42	0.064	-	0.010	-	2.04	-	0.96	40±18	81±27	0.010	6.7	7.34	fd					
HIJASS J1230+42	0.097	-	0.012	-	11.09	-	2.00	151±14	192±21	0.011	6.3	8.01	fc5					
HIJASS J1230+41	2.324	2.019	0.108	0.108	361.91	414.95	9.27	175±8	241±12	0.038	8.9	9.89	ecd					
HIJASS J1231+29	0.146	0.131	0.017	0.017	8.77	9.81	2.36	67±8	80±12	0.016	9.2	8.29	e					
HIJASS J1232+39	0.140	-	0.012	-	4.35	-	0.95	33±8	56±12	0.010	10.4	8.04	db					
HIJASS J1232+42	0.249	0.226	0.021	0.021	16.77	18.65	2.78	80±8	101±12	0.018	8.5	8.50	eb					
HIJASS J1232+37	0.233	0.211	0.024	0.024	29.4	32.76	4.67	181±12	212±18	0.022	7.7	8.66	e					
HIJASS J1232+31	0.610	0.543	0.034	0.034	37.5	42.22	3.00	61±4	78±6	0.020	4.9	8.37	ei					
HIJASS J1233+32	0.089	0.080	0.014	0.014	5.81	6.49	1.99	73±18	109±27	0.013	13.3	8.44	ec5					
HIJASS J1233+33	0.083	0.074	0.014	0.014	2.42	2.73	1.34	30±24	76±36	0.013	12.1	7.97	e					
HIJASS J1233+24	0.068	0.060	0.015	0.015	2.05	2.34	1.59	32±32	80±48	0.015	18.4	8.27	e					
HIJASS J1233+39	0.108	-	0.011	-	3.26	-	0.93	33±8	50±12	0.010	10.0	7.89	d					
HIJASS J1233+30	0.081	0.075	0.014	0.014	8.68	9.55	2.50	149±22	195±33	0.013	16.8	8.80	e					
HIJASS J1234+39	0.105	-	0.012	-	7.85	-	1.62	76±8	92±12	0.011	10.3	8.29	e					
HIJASS J1234+35	0.692	0.617	0.036	0.036	66.77	75.07	3.38	122±4	139±6	0.018	11.8	9.39	e					
HIJASS J1235+41	0.065	-	0.011	-	1.78	-	0.89	31±12	47±18	0.010	9.4	7.57	e					
HIJASS J1235+27	1.566	1.380	0.073	0.073	273.75	310.4	5.87	242±4	257±6	0.023	11.5	9.99	ec					
HIJASS J1236+25	1.292	1.127	0.062	0.062	272.72	311.65	7.36	497±6	523±9	0.026	12.0	10.02	eci					
HIJASS J1236+40	0.172	0.155	0.020	0.020	24.25	27.1	4.05	190±10	206±15	0.018	8.1	8.63	e					
HIJASS J1238+32	0.485	0.435	0.026	0.026	13.79	15.45	1.52	29±4	44±6	0.015	3.8	7.73	ei					
HIJASS J1239+44	0.193	0.175	0.020	0.020	7.32	8.14	2.09	38±8	55±12	0.018	8.9	8.18	e					
HIJASS J1240+32	0.079	-	0.008	-	5.58	-	1.00	75±12	113±18	0.007	11.1	8.21	df					
HIJASS J1241+41	1.050	0.911	0.052	0.052	110.61	126.98	5.22	136±6	179±9	0.026	8.7	9.36	ec					
HIJASS J1242+32	1.848	-	0.094	-	449.62	-	3.98	298±4	324±6	0.015	7.3	9.75	cdi					
HIJASS J1242+38	0.522	0.469	0.036	0.036	23.65	26.48	3.45	47±6	62±9	0.027	4.6	8.11	ei					
HIJASS J1243+24	0.047	-	0.010	-	4.62	-	1.69	115±12	124±18	0.010	25.8	8.86	f					
HIJASS J1243+32	2.050	-	0.103	-	255.85	-	2.28	134±6	184±9	0.012	9.4	9.73	cd					
HIJASS J1244+34	0.246	0.223	0.016	0.016	13.13	14.62	1.65	58±4	72±6	0.012	9.0	8.44	eb					

Table 3 – Continued

HIJASS name (B1)	$S_p$ Jy (B2)	$S_p(\text{corr})$ Jy (B3)	$\sigma_{\text{peak}}$ Jy (B4)	$S_{\text{int}}$ Jy $\text{km s}^{-1}$ (B5)	$S_{\text{int}}(\text{corr})$ Jy $\text{km s}^{-1}$ (B6)	$\sigma_{\text{int}}$ Jy $\text{km s}^{-1}$ (B7)	$w_{50} \pm \sigma_{50}$ $\text{km s}^{-1}$ (B8)	$w_{20} \pm \sigma_{20}$ $\text{km s}^{-1}$ (B9)	rms Jy (B10)	Distance Mpc (B11)	$\log M_{\text{HI}}$ (B12)	flags <sup>a</sup> (B13)
HIJASS J1244+28	0.079	0.070	0.011	4.87	5.49	1.51	71±12	92±18	0.010	13.4	8.37	e
HIJASS J1245+27	0.105	0.097	0.015	9.82	10.81	2.52	102±20	157±30	0.014	15.3	8.78	ec
HIJASS J1246+36	0.554	0.493	0.038	19.02	21.41	3.25	33±6	55±9	0.029	3.0	7.65	ei
HIJASS J1250+25	0.508	-	0.027	101.09	-	1.92	382±6	413±9	0.008	12.4	9.56	di
HIJASS J1250+41	0.581	0.504	0.042	98.67	113.17	8.42	210±8	239±12	0.033	4.4	8.71	ei
HIJASS J1251+26	0.069	-	0.009	3.36	-	0.95	51±14	87±21	0.008	17.7	8.39	df
HIJASS J1251+25	0.402	-	0.023	32.19	-	1.68	78±10	176±15	0.011	17.1	9.34	d
HIJASS J1254+27	1.037	0.911	0.051	90.71	103.07	4.16	92±4	110±6	0.023	4.0	8.60	ei

<sup>a</sup> Flags for extended (e) and confused (c) HI sources, HI sources without a central position from a position fit (f), newly detected sources in the 21-cm emission line (n), HI sources lying nearby negative bandpass sidelobes (b), DUCHAMP double detections (d), HI sources with systemic velocities below 300  $\text{km s}^{-1}$  (v) and sources with independent distance measurements available (i). Numbers indicate HI sources with higher order baseline fits to their spectra.

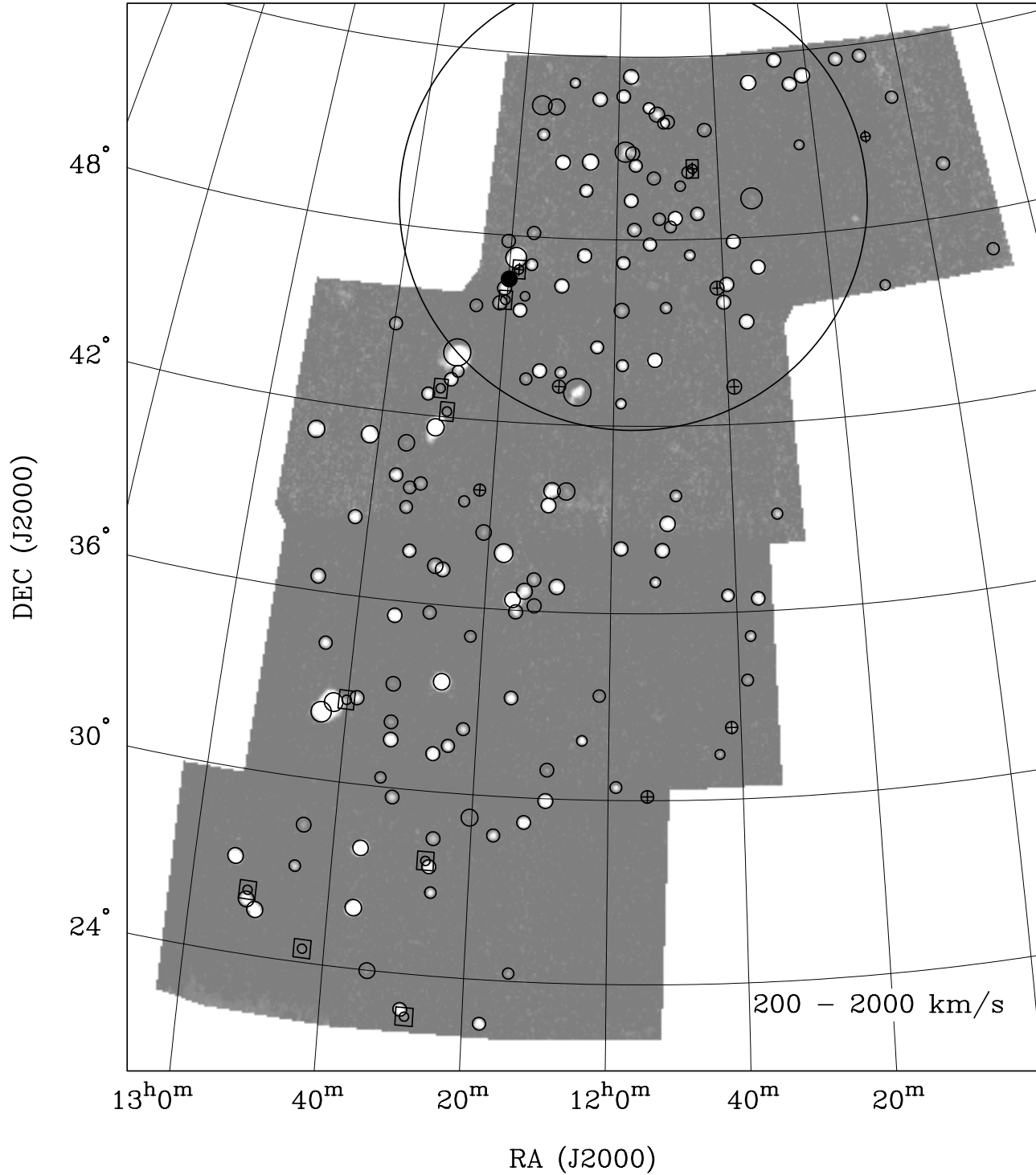


**Figure 3.** Velocity integrated H I distribution of the Ursa Major region as obtained from the HIJASS data (grey scale). The large circle (with radius 7.5 deg) drawn in the northern part shows the projected position of the Ursa Major cluster as defined by Tully et al. (1996). Overlaid are symbols to indicate the projected positions and sizes of H I detections as presented in this catalogue - open circles indicate H I sources with an associate optical counterpart whereas the filled circle marks the candidate galaxy/H I cloud, HIJASS J1219+46. This source and the H I detections marked with crosses are newly detected in the 21-cm emission line. Circles surrounded by boxes indicate H I detections for which no central position and no extent (major and minor axis) is measurable.

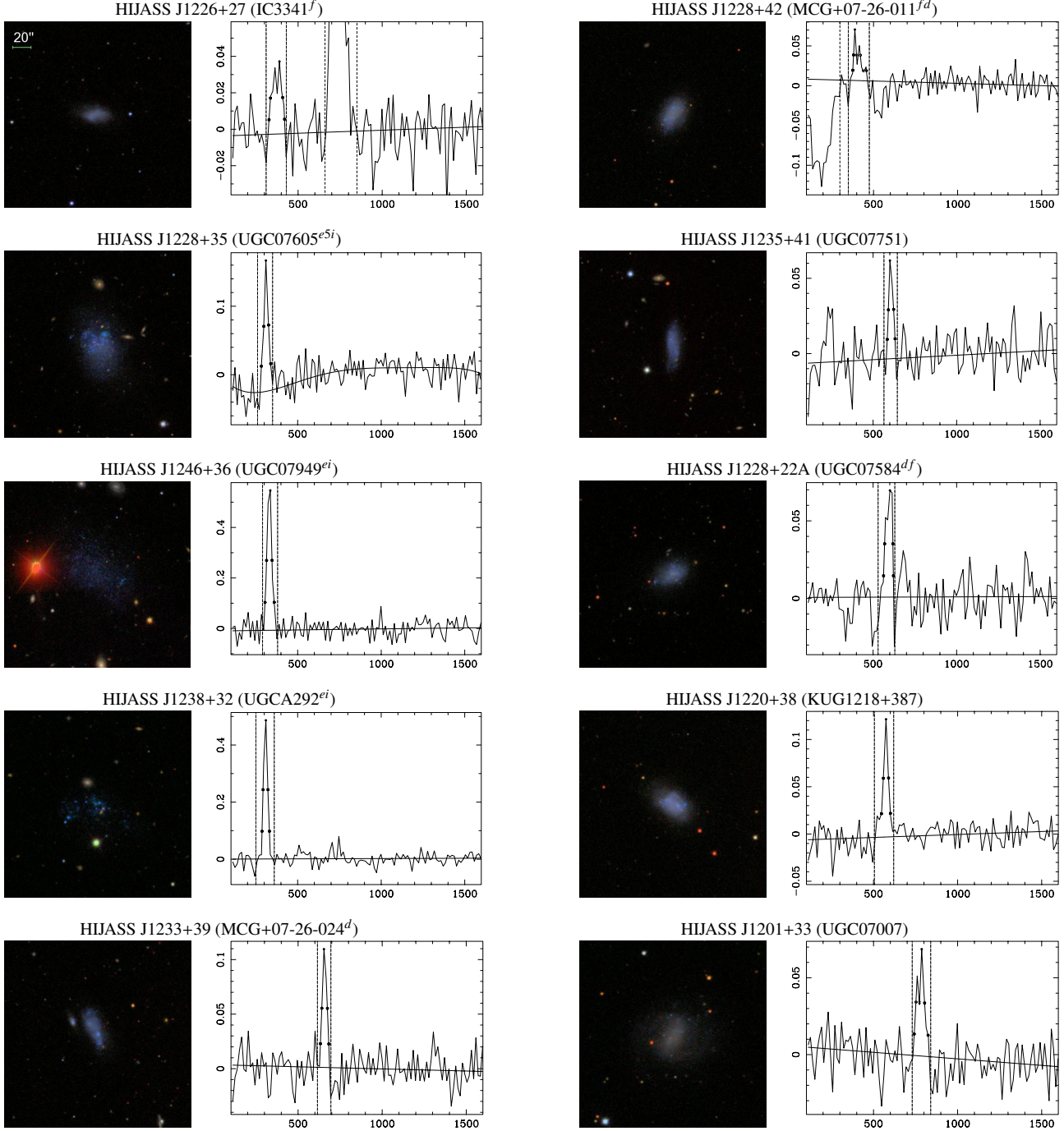


**Figure 4.** Multi-colour SDSS images of the lowest HI mass and previously catalogued galaxies with systemic velocities between  $300$  and  $1900 \text{ km s}^{-1}$  together with the HIJASS spectra. The HI masses increase from the left to the right and from the top to the bottom – note that we do not show HIJASS J1218+46 with an HI mass between the ones of HIJASS J1228+22A and HIJASS J1238+32 as it is shown in Figure 5. The HIJASS name along with the most likely optical counterpart (in brackets) is given above each SDSS image and spectrum (including the flags as discussed in Section 3.2). The SDSS images ( $3.3' \times 3.3'$ ) are centered on the optical positions of the most likely counterparts. The HI spectra have the optical velocities ( $cz$  in  $\text{km s}^{-1}$ ) along the abscissas and the flux densities (in Jy) along the ordinates. The HI line emission analysis is conducted within the velocity range as indicated by the dotted vertical lines. The baseline fits to the spectra are conducted within the displayed velocity range excluding the velocity ranges of HI line emission analysis and of other HI sources (e.g. NGC4393 at  $\sim 650\text{--}850 \text{ km s}^{-1}$  in the spectra of HIJASS J1226+27). Note that we show the HI spectra prior to baseline subtraction. Hence, the marked HI peak flux as well as the 50 and 20 per cent velocity widths slightly vary from the values given in the catalogue as they are measured after baseline subtraction.

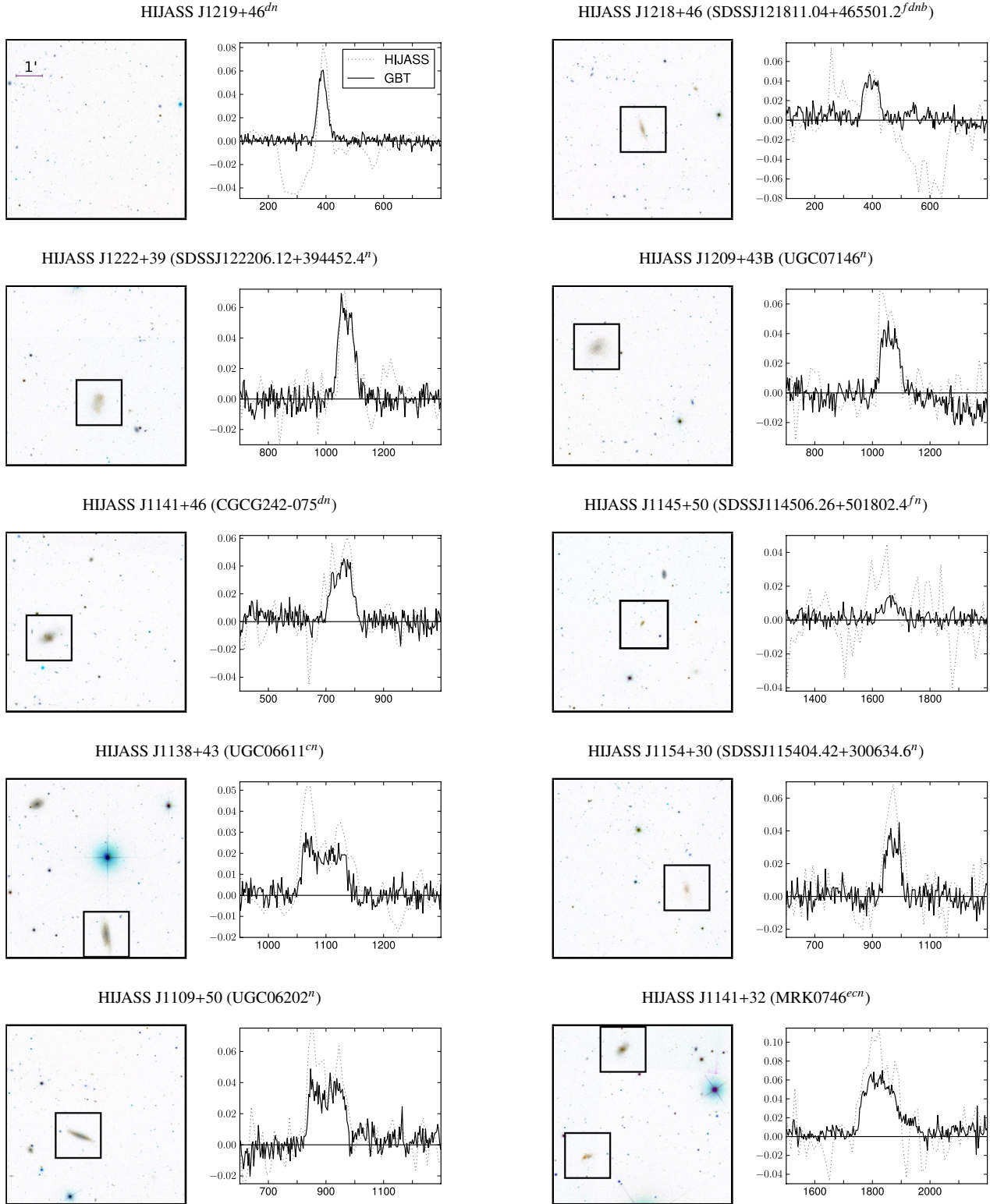


**Figure 5. The first time detections in the 21-cm emission, including the candidate galaxy/HI cloud, HIJASS J1219.** We show the inverted multi-colour SDSS images ( $\sim 7' \times 7'$ ) together with the HIJASS and GBT spectra ordered with increasing HI mass (similar to Figure 4). (*left*) The SDSS images are centered on the HI positions, and the optical counterparts are marked with boxes. There is no obvious optical counterpart apparent in the SDSS image of HIJASS J1219+46. (*right*) For comparison, we show the GBT spectrum on top of the HIJASS spectrum (after baseline subtraction). The spectra have the optical velocities ( $cz$  in  $\text{km s}^{-1}$ ) along the abscissas and the flux densities (in Jy) along the ordinates. The velocity range of the HI line emissions as well as the negative troughs in the HIJASS spectra of HIJASS J1219+46 ( $220\text{--}360 \text{ km s}^{-1}$  dotted/grey) and HIJASS J1218+46 ( $430\text{--}700 \text{ km s}^{-1}$  dotted/grey) are excluded from the baseline fits. HIJASS J1141+32 is further discussed in Section 4.3. Note that we show the spectra of HIJASS J1219+46 and HIJASS J1138+43 3-point Hanning smoothed.

### 3.4 Candidate galaxy/HI cloud

The presented catalogue of 166 H I sources in the Ursa Major region contains 162 H I detections, which are clearly associated with previously catalogued galaxies as listed in the NASA/IPAC Extragalactic Database (NED – with cross-identifications) or the Sloan Digital Sky Survey (SDSS DR8 – redshift confidence level  $z_{conf} > 0.95$ ). Another three HIJASS detections – namely HIJASS J1226+27, HIJASS J1243+24 and HIJASS J1233+24 – can be matched up with H I sources listed in the ALFALFA 40 per cent catalogue (Haynes et al. 2011) and have been assigned to IC3341, KUG1240+247 and MAPS-NGP O\_378\_0206985 respectively. Note that HIJASS J1233+24 was first catalogued in Lang et al. (2003) using the same HIJASS data set and is therefore listed in NED (without cross-identifications). Therefore, only one H I detection – HIJASS J1219+46 – does not have a previously catalogued optical counterpart with known velocity listed in NED, SDSS or ALFALFA (HIJASS J1219+46 lies outside the ALFALFA declination range).

To identify a potential optical counterpart of the candidate galaxy/H I cloud we investigate SDSS and Digitized Sky Survey (DSS) images. We compare the images centered on the central position of HIJASS J1219+46 to the ones of the lowest H I mass and previously catalogued galaxies in the sample (see Figure 4). One might expect that the candidate dwarf galaxy has a similar optical counterpart as the known galaxies within the same mass bin – however, as it has not been previously catalogued one might also expect it to have lower surface brightness and thus be less easily visible. All of the lowest H I mass galaxies show faint patches of nebulosity in the multi-colour SDSS images (Figure 4). Furthermore, we show HIJASS sources that are newly detected in the 21-cm emission line in Figure 5. These SDSS images are centred on the H I position and therefore show typical offsets from the optical counterparts. For clarification we invert the colours of the multi-colour SDSS images in Figure 5 (as opposed to Figure 4). We do not find a similar galaxy in the images for HIJASS J1219+46 within the search radius (the position uncertainty is 1.2 arcmin as given in Table 2). There are multiple galaxies listed in SDSS with no redshift measurements, which match in position to the candidate galaxy/H I cloud. To determine the optical counterpart(s) and/or confirm the H I cloud accurate position is required from follow-up observations. It is also quite possible that deeper optical imaging is required to determine any optical counterparts.

In Figure 6 we show a 1.4 deg  $\times$  1.4 deg DSS B-band image of the candidate galaxy/H I cloud and its surroundings with overlaid H I intensity contours integrated over the velocity range from 360 to 430 km s<sup>-1</sup>. HIJASS J1219+46 is a confused source in the DUCHAMP output with HIJASS J1220+46/NGC4288. The angular separation to NGC4288 is 0.3 deg, which corresponds to a distance of  $\sim$ 40 kpc assuming that the region lies at a distance of 7.6 Mpc. To the north of HIJASS J1219+46 lies HIJASS J1218+46 (SDSSJ121811.04+465501.2) and HIJASS J1218+47/M106 (including NGC4248, UGC07356 and two SDSS galaxies). The angular separation to M106 is 0.7 deg, which corresponds to  $\sim$ 93 kpc. Although, HIJASS J1219+46 lies nearby negative bandpass sidelobes emerging from HIJASS J1218+47/M106 the Green Bank Telescope follow-up observations confirm the H I properties measured in HIJASS as given in Table 4 (the GBT and HIJASS spectra are shown in Figure 5 – the negative bandpass sidelobes are apparent at 220 to 360 km s<sup>-1</sup> in the HIJASS spectrum). The na-

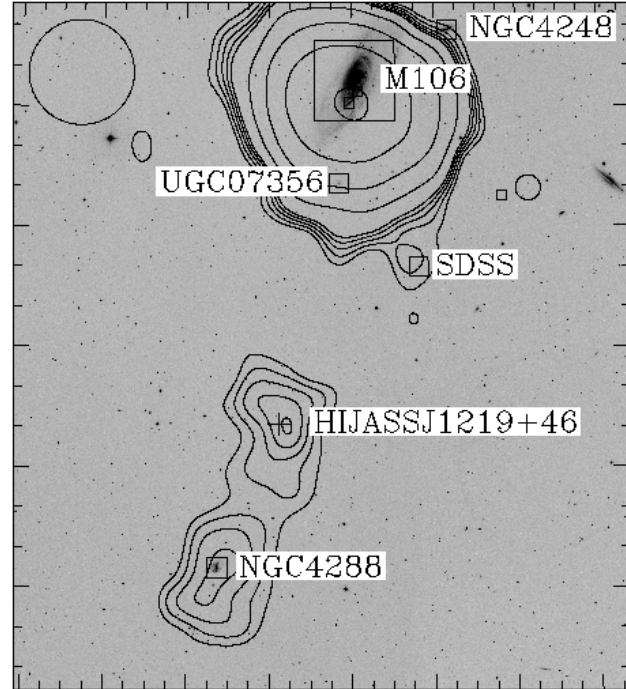


**Figure 6.** Candidate galaxy/H I cloud found in the HIJASS data – HIJASS J1219+46 (indicated by a cross and labelled in the Figure). We show a DSS blue image (1.4 deg  $\times$  1.4 deg) with overlaid H I intensity contours at 1, 1.5, 2, 2.5, 3, 6, 12, 24 and 48 Jy beam<sup>-1</sup> km s<sup>-1</sup> integrated over the velocity range from 360 to 430 km s<sup>-1</sup>. The gridded beam is displayed in the top left corner (FWHM 13.1 arcmin). Galaxies residing in this region are marked with boxes and some are labelled in the Figure.

ture of HIJASS J1219+46 could be tidally stripped gas or a dwarf companion.

Wilcots et al. (1996) observed NGC4288 using the Very Large Array (D-configuration; channel width of 5.2 km s<sup>-1</sup> and a rms noise of 1.0 mJy beam<sup>-1</sup>) finding a gas cloud to the south of NGC4288 (also see Kovač et al. 2009). Furthermore, the gas cloud shows a tidally disrupted H I stream that extends well beyond the optical disk of NGC4288 (Wilcots et al. 1996) towards HIJASS J1219+46. However, HIJASS J1219+46 lies just outside the area covered by Wilcots et al. (1996) and Kovač et al. (2009).

### 3.5 Comparison of measured HI parameters with values in the literature and follow-up observations

We find 165 H I sources with one or more associate optical counterparts as listed in NED and SDSS in the HIJASS data. For H I detections with *one, clear* associate counterpart, i.e. H I sources that are not confused (c), not double detections (d) and not in the vicinity of negative bandpass (b) sidelobes (as labelled in this catalogue in Section 3.2), we show the position and velocity offsets from our measured H I parameters to previously obtained H I parameters in Figure 7. We compare our results to recent literature values: (i) Verheijen & Sancisi (2001) extensively studied 43 spiral galaxies in the Ursa Major cluster using WSRT, (ii) Springob et al. (2005) have compiled a homogenous sample of H I properties of more than 9000 galaxies from single dish observations, (iii) Kovač et al. (2009) have conducted a blind H I survey in the Canes Venatici region using the WSRT and (iv) the ongoing ALFALFA

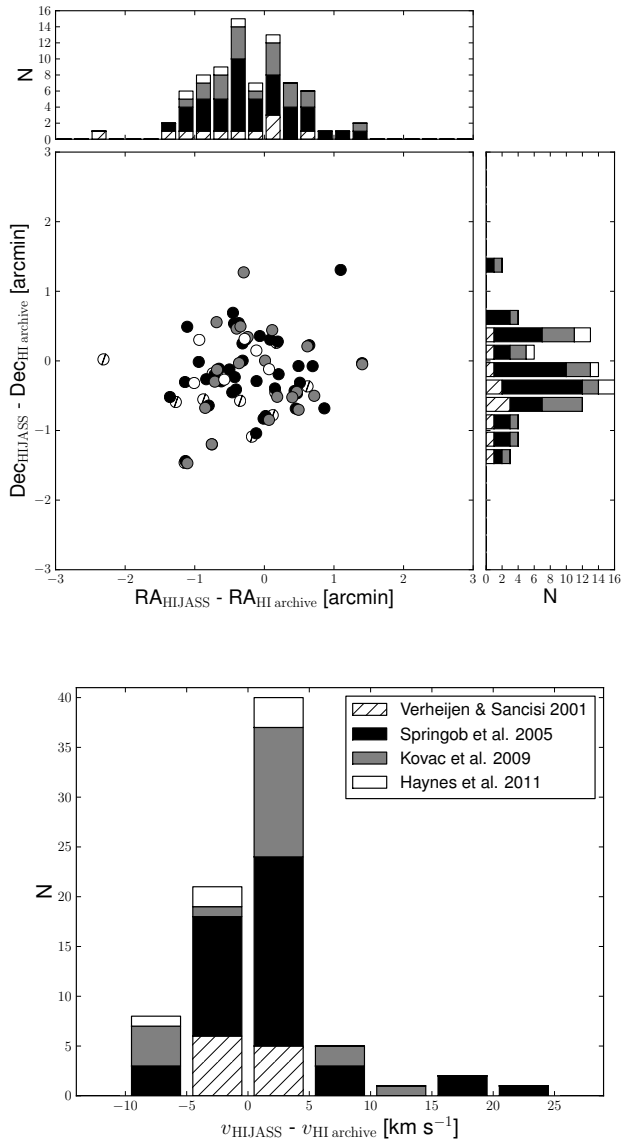


**Figure 7.** The differences between H I parameters as listed in this paper and previously obtained H I parameters (the used literature is noted in the key) for H I sources with only *one* associate optical counterpart within the gridded beam size and the velocity range of the H I source. (*Top*) the position offsets; (*bottom*) the systemic velocity offsets – the comparison to Kovač et al. (2009) uses local group velocities as discussed in Yahil et al. (1977).

survey using the Arecibo covers a strip in the southern part of the region ( $+24^\circ \leq \delta \leq +28^\circ$ ) (Haynes et al. 2011). The congruent sample of clear H I sources in this study and the literature includes 78 galaxies. The central positions and velocities presented in this paper are generally consistent with the literature values within the errors (see Figure 7).

In Figure 8 we compare the integrated fluxes measured in HIJASS to recent literature values as well as the GBT follow-up observations listed in Table 4. We show a comparison of the percentage difference of integrated fluxes measured in HIJASS to the ones in the literature and with the GBT (*top*) as well as the comparison of the absolute flux values for the sample (*bottom*). The

percent difference is calculated as follows:

$$\% \text{Diff} = \frac{S_{\text{int}}(\text{HIJASS}) - S_{\text{int}}(\text{HI archive, GBT})}{S_{\text{int}}(\text{HI archive, GBT})} \times 100$$

Some integrated fluxes differ by more than 20%, in particular in comparison to Kovač et al. (2009). This may be explained as they use an interferometric dataset (obtained with WSRT) which is not sensitive to diffuse H I emission compared to a single-dish observation.

There are some data points that lie outside the displayed range in Figure 8 (*top*): HIJASS J1254+27/NGC4789A with  $\text{Diff} = 219\%$  in comparison with Springob et al. (2005). We find a wide range of literature values for this dwarf irregular galaxy. NGC4789A has a large H I to optical radius ratio (Hoffman et al. 1996), therefore some telescopes may resolve out significant flux. There are two outliers in comparison with the GBT follow-up observations – HIJASS J1218+46/SDSSJ121811.04+465501.2 ( $\text{Diff} = 152\%$ ) and HIJASS J1145+50/SDSSJ114506.26+501802.4 ( $\text{Diff} = 202\%$ ). See Figure 5 for the comparison of the GBT and HIJASS spectra. HIJASS J1218+46 is a double detection with HIJASS J1218+47 including M106, UGC07356, NGC4248 and two SDSS galaxies (also see Figure 6). Given that the angular separation between SDSSJ121811.04+465501.2 and M106 is 24.5 arcmin and the angular separation between SDSSJ121811.04+465501.2 and UGC07356 is 14.4 arcmin, these galaxies may contribute a significant amount of flux to the HIJASS detection (FWHM 13.1 arcmin) in comparison to the GBT observation (FWHM 9 arcmin). Regarding SDSSJ114506.26+501802.4, the mean signal-to-noise ratio in the HIJASS data is only 1.5 – therefore the rms noise contributes significantly to the measured integrated H I flux in comparison to the GBT data. In general, this literature comparison shows that H I properties of galaxies measured with different telescopes and obtained with different parametrization procedures lead to consistent results within the errors. However, for H I detections near the detection limit, the noise can cause fluctuations in the H I measurements.

## 4 DISCUSSION AND RESULTS

### 4.1 Velocity Distribution

The velocity distribution of galaxies residing in the Ursa Major region is shown in Figure 9. The top panel shows the velocity distribution of galaxies as listed in SDSS (white) with spectroscopic redshifts with confidence levels  $z_{\text{conf}} > 0.95$  and additional galaxies listed in NED (grey) with cross-identifications. To avoid duplicates we cross-correlate the galaxies listed in NED and SDSS within 1 arcmin and 50 km s<sup>-1</sup> of the central position and velocity. The bottom panel shows the velocity distribution of the H I selected galaxies as catalogued in this paper with systemic velocities between 300 and 1900 km s<sup>-1</sup>. The H I detections are colour-coded according to H I sources with associate optical counterparts (in grey) and the previously uncatalogued candidate galaxy/H I cloud (in black).

One can see the large scale structure of the region - the over-density appearing at  $\sim 950$  km s<sup>-1</sup> in the optical and (less clearly) in the H I selected sample indicates the presence of the Ursa Major cluster. There are 212 galaxies listed in SDSS and NED within the Ursa Major cluster definition by Tully et al. (1996). In this paper we present 51 H I detections within the cluster definition by



**Table 4.** The HI properties of newly detected HI sources as measured with the GBT.

HIJASS name (A1)	$v_{\text{sys}} \pm \sigma_v$ km s <sup>-1</sup> (A5)	$S_p$ Jy (B2)	$\sigma_{\text{peak}}$ Jy (B4)	$S_{\text{int}}$ Jy km s <sup>-1</sup> (B5)	$\sigma_{\text{int}}$ Jy km s <sup>-1</sup> (B7)	$w_{50} \pm \sigma_{50}$ km s <sup>-1</sup> (B8)	$w_{20} \pm \sigma_{20}$ km s <sup>-1</sup> (B9)	rms Jy (B10)
HIJASS J1109+50	905 ± 2	0.049	0.006	4.63	0.36	132 ± 4	146 ± 6	0.005
HIJASS J1138+43	1190 ± 2	0.030	0.004	3.22	0.28	155 ± 4	171 ± 6	0.004
HIJASS J1141+46	755 ± 3	0.045	0.006	3.24	0.33	75 ± 6	105 ± 9	0.005
HIJASS J1141+32	1852 ± 4	0.070	0.008	8.29	0.55	123 ± 8	198 ± 12	0.007
HIJASS J1145+50	1663 ± 8	0.015	0.005	0.82	0.27	68 ± 16	105 ± 24	0.005
HIJASS J1154+30	972 ± 2	0.045	0.007	2.01	0.31	60 ± 4	72 ± 6	0.006
HIJASS J1209+43B	1061 ± 3	0.049	0.007	2.81	0.38	69 ± 6	90 ± 9	0.007
HIJASS J1218+46	398 ± 2	0.047	0.006	2.48	0.30	62 ± 4	75 ± 6	0.006
HIJASS J1219+46	390 ± 1	0.061	0.004	2.29	0.14	36 ± 2	56 ± 3	0.003
HIJASS J1222+39	1071 ± 2	0.069	0.006	3.71	0.28	59 ± 4	81 ± 6	0.005

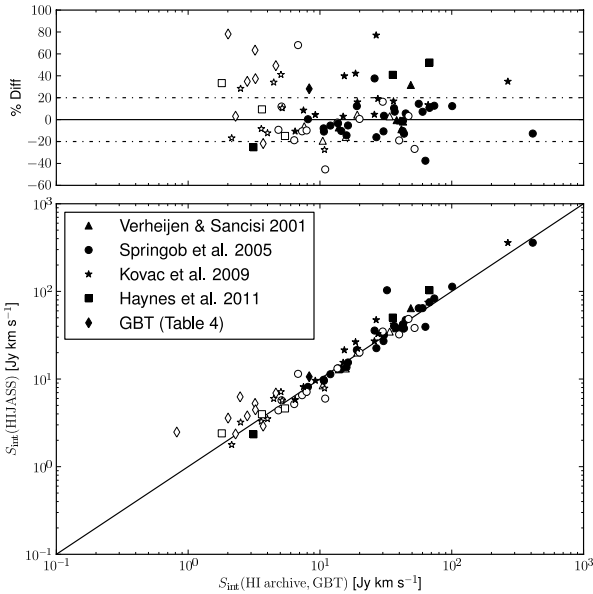


**Figure 8.** Comparison of integrated fluxes measured in HIJASS with values in the literature and measured with the GBT (follow-up observations): (top) deviation of values measured in HIJASS compared to the ones in the literature and obtained with the GBT; (bottom) the integrated flux values from the literature and the GBT plotted against the ones measured in HIJASS. The used literature is noted in the key. The light coloured markers represent point sources; the dark ones are for extended sources as listed in the catalogue (Table 3). The solid lines mark the unity relationship and the dashed lines (top panel) limit the 20 per cent difference in the integrated flux measurements.

Tully et al. (1996) that contain 96 previously catalogued galaxies. The high number of confused detections in our data is due to a high density of galaxies in the cluster. We will discuss cluster/group membership, substructures and HIJASS non-detections in a forthcoming paper but the number of high-probability cluster members is likely to increase significantly from the 79 cluster members identified in Tully et al. (1996).

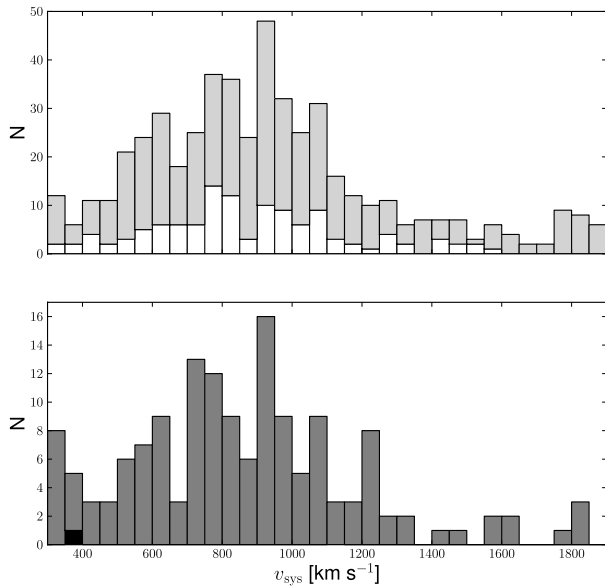
There are many groups nearby the cluster, which overlap and make the cluster difficult to define. In particular foreground galaxy groups with velocities  $v < 700$  km s<sup>-1</sup> lead to an asymmetric galaxy distribution in the optical and HI selected sample. The number of galaxies with velocities  $v > 1300$  km s<sup>-1</sup> is lower than the number of galaxies residing in the foreground. This may be a selection effect or could indicate the filamentary structure: the Ursa Major cluster (at 17.1 Mpc) is connected with the Virgo cluster (at ~16 Mpc Mei et al. 2007) via the galaxies and galaxy groups lying at the low velocity end.

Figure 9 also shows one nearby candidate galaxy/HI cloud. We find no candidate galaxies/HI clouds in the Ursa Major cluster, where one might expect to find some e.g. due to previously uncatalogued gas-rich dwarf irregular galaxies or the presence of stripped HI gas. Given that our HI mass limit at the distance of the Ursa Major cluster is  $2.5 \times 10^8 M_{\odot}$  (assuming a velocity width of 100 km s<sup>-1</sup>) we cannot rule out candidate galaxies/HI clouds below the HI mass limit.

## 4.2 HI Mass Distribution

Figure 10 shows the HI mass distribution of 151 HI sources as listed in this catalogue (excluded are 15 galaxies with central velocities below 300 km s<sup>-1</sup>). HI sources that have been previously detected and are listed in NED/SDSS are shown in grey whereas the candidate galaxy/HI cloud is presented in black. The latter inhabits the low HI mass end and is likely to be a dwarf galaxy, i.e. of the same galaxy population as the previously catalogued galaxies within the same mass bin. Taylor & Webster (2005) note that ‘dark’ (optically invisible) HI galaxies are unlikely to be detected in our studied mass range between  $10^7$  and  $10^{10.5} M_{\odot}$  as the HI gas is normally associated with star formation or is destroyed. Meurer et al. (2006) also find that dormant (non-star-forming) galaxies with HI masses above  $3 \times 10^7 M_{\odot}$  are very rare. However, high resolution follow-up observations are required to determine the nature of HIJASS J1219+46. We discussed the candidate galaxy/HI cloud in more detail in Section 3.4. We note that we did not find a numerous low-mass population of gas-rich dwarf galaxies to solve the dwarf deficiency problem as discussed in Trentham et al. (2001).

We can place an upper limit on the HI mass for the galaxies listed in NED/SDSS within the Ursa Major region, which we did



**Figure 9.** Velocity distribution of galaxies residing in the Ursa Major region: (*top*) galaxies as listed in SDSS (white) and additional galaxies listed in NED (grey); (*bottom*) H I selected galaxies as catalogued in this paper with an associate optical counterpart coloured in grey whereas the nearby candidate galaxy/H I cloud is shown in black.

not detect in HIJASS. The survey sensitivity is  $2.5 \times 10^8 M_{\odot}$  (assuming a velocity width of  $100 \text{ km s}^{-1}$  and a distance of  $17.1 \text{ Mpc}$ ). A lower H I mass limit is valid for galaxies lying in the foreground groups and filamentary structure (with  $v < 700 \text{ km s}^{-1}$  and distances  $D < 17.1 \text{ Mpc}$ ), whereas for background galaxies ( $v > 1200 \text{ km s}^{-1}$ ) with distances  $D > 17.1 \text{ Mpc}$  a slightly higher H I mass limit is appropriate (as  $M_{\text{HI}} = 8.38 \times 10^5 \times D^2$ ).

### 4.3 Candidates for galaxy-galaxy interactions

In this paper, there are 54 H I detections (33 per cent) which have two or more optical counterparts as listed in NED/SDSS within the gridded beam size and within the velocity range of the H I detection (see H I detections labelled with ‘c’ in the catalogue in Section 3.2). We can not clearly associate the H I content with only one optical counterpart. However, these H I detections with multiple optical counterparts are intriguing objects as galaxy-galaxy interactions might take place due to the small separation between the galaxies (e.g.  $10 \text{ arcmin}$  corresponds to  $50 \text{ kpc}$  at a distance of  $17.1 \text{ Mpc}$ ).

For example, **HIJASS J1141+32** encompasses four previously known dwarf galaxies within  $1700$  and  $1900 \text{ km s}^{-1}$  (see Figure 11): MRK0746, KUG1138+327, WAS28 and SDSSJ114135.98+321654.0 (which has no cross-identification in NED and is therefore not listed in our catalogue) – there are no previous detections in the 21-cm emission line for any of these galaxies. High resolution follow up observations are required to study the H I distribution, kinematics and possible interaction of these galaxies.

**HIJASS J1220+29** encompasses three previously catalogued galaxies (see Figure 11) at  $610 - 710 \text{ km s}^{-1}$ , namely NGC4278 (elliptical), SDSSJ122005.73+291650.0 (spiral) and

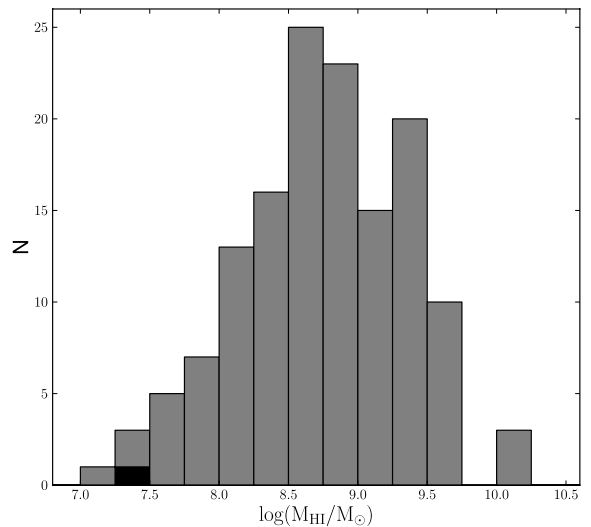


**Figure 10.** The H I mass histogram of the catalogued sources in this paper with systemic velocities between  $300$  and  $1900 \text{ km s}^{-1}$ . Grey shadings correspond to H I sources with an associate optical counterpart whereas the candidate galaxy/H I cloud is shown in black.

NGC4286 (spiral) (ordered with increasing angular separation from the central H I position). Morganti et al. (2006) have conducted a WSRT observation of NGC4278, NGC4286 and SDSSJ122005.73+291650.0 – the observations reveal two tail-like structures west and south-west of NGC4278.

Out of the 54 confused HIJASS detections, 33 galaxies appear to have dwarf companions (one or two small objects as listed in SDSS, 2MASX, SBS, MCG, HS, CGCG). This leaves us with 21 high-probability candidates for galaxy-galaxy interactions of which 11 HIJASS detections (52 per cent) are within the Ursa Major cluster as defined by Tully et al. (1996). It is remarkable that the Ursa Major cluster as defined by Tully et al. (1996) only comprises approximately 12 per cent of the surveyed volume discussed in this paper but contains about half of all high-probability candidates for galaxy-galaxy interactions. This is also the case (48 per cent) if we include two nearby DUCHAMP double detections, i.e. we do not only consider galaxies within the gridded beam (as the physical size of the beam is smaller for nearby regions) but also merged H I detections as candidates for high-probability galaxy-galaxy interactions. Verheijen & Sancisi (2001) have observed 10 of the high-probability candidates for galaxy-galaxy interactions in the Ursa Major cluster. The sample includes the most massive galaxy (Messier109), the largest (NGC3718) and some of the brightest systems (NGC4026, NGC4111 and NGC4088).

According to Verheijen & Sancisi (2001) the interacting systems are: (i) **NGC3769** is strongly interacting with its dwarf companion NGC3769A. (ii) **NGC3893** is an interacting pair with NGC3896. (iii) Some tidal debris can be seen in the interacting pair **IC0750** and **IC0749**. (iv) The largest galaxy in the cluster – **NGC3718** – shows distorted morphology and may be interacting with NGC3729. (v) **NGC4088** is one of the brightest systems in the Ursa Major cluster with ongoing vigorous star formation. The system is strongly disturbed and in close vicinity of NGC4085.

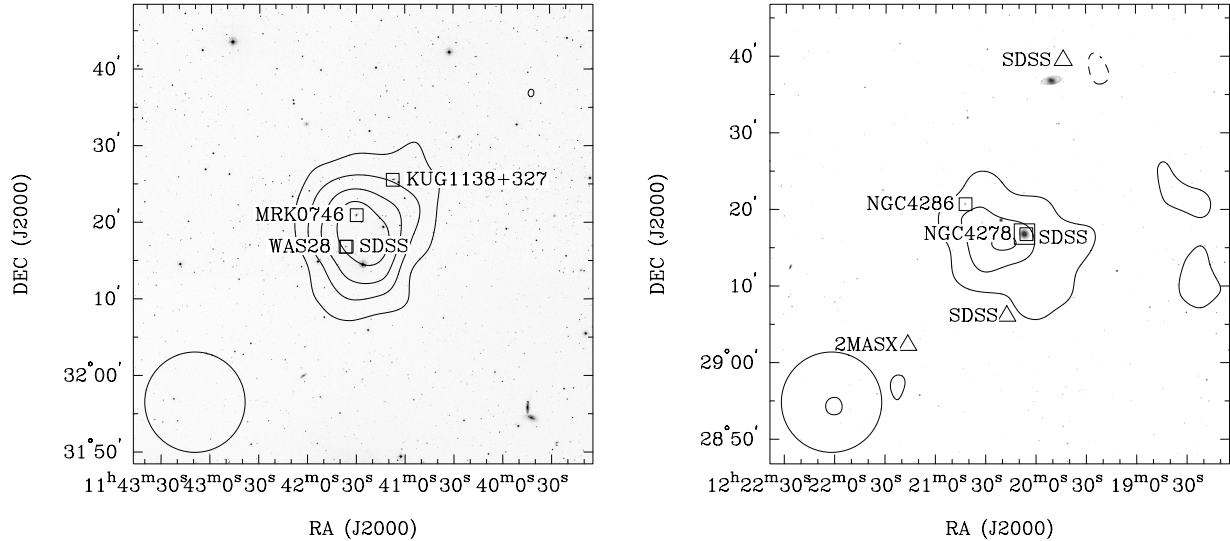


**Figure 11.** Two candidate regions for galaxy-galaxy interactions are shown with DSS2 B-band images ( $1^\circ \times 1^\circ$ ) and overlaid integrated flux levels (contours) starting at  $\pm 1.5 \text{ Jy beam}^{-1} \text{ km s}^{-1}$ . Negative contour levels are indicated with dashed lines. The gridded beam size is indicated in the bottom left corner of each image. (*left*) HIJASS J1141+32: There are four dwarf galaxies at approximately  $1700 - 1900 \text{ km s}^{-1}$  as indicated by boxes and labelled in the Figure. The increment of the contour levels is  $2 \text{ Jy beam}^{-1} \text{ km s}^{-1}$ . (*right*) HIJASS J1220+29: The NGC4278 group at approximately  $400 - 850 \text{ km s}^{-1}$ . The contour lines include three previously catalogued galaxies as listed in NED (marked with boxes and labelled in the Figure) and increase with  $1 \text{ Jy beam}^{-1} \text{ km s}^{-1}$ . We also show three galaxies (at similar velocities than the NGC4278 group) that are not detected in HIJASS (triangles).

(vi) The NGC4111 and (vii) NGC4026 groups are also known to be interacting and discussed in more detail in Section 4.4.

Three of the high-probability candidates – namely NGC3917, Messier109 and NGC4157 – do not show any signs of interactions with their dwarf companions (Verheijen & Sancisi 2001).

Verheijen & Sancisi (2001) find further interacting galaxy pairs: NGC3949 may be interacting with a small companion (SDSSJ115340.69+475156.4) and UGC06818 may be tidally interacting with a faint companion – these systems are not included in our sample of high-probability candidates for galaxy-galaxy interactions as they include interactions with dwarf companions. Note that we quote UGC06818 as a clear single detection in our catalogue – there are no galaxies listed in close vicinity of UGC06818 in NED/SDSS with known redshifts. Verheijen & Sancisi (2001) also find NGC3998 with disturbed HI content, which lies just outside the HIJASS data cubes at Dec.  $\delta \approx 55^\circ 27' 13''$ .

#### 4.4 HIJASS detections with extended HI envelopes

We find two HI detections with extended HI envelopes that do not have previously catalogued galaxies within the HI extension.

Within the Ursa Major cluster lies the HI extension/plume in the NGC4026 group (see Figure 12), which has already been studied by Appleton (1983; Jodrell Bank), van Driel et al. (1988; WSRT) and Verheijen & Zwaan (2001; VLA D-array). Six galaxies are listed in NED with heliocentric velocities  $700 \leq v \leq 1100 \text{ km s}^{-1}$ , four of which are included in the HI envelope (boxes) and two of which are in vicinity of the HI extensions (triangles; non-detection in HIJASS). The WSRT observations reveal an HI filament at  $\alpha \approx 11^h 58^m 57^s$  and  $\delta \approx 50^\circ 46' 42''$  with a systemic velocity of  $\sim 960 \text{ km s}^{-1}$  (van Driel et al. 1988). The HI filament measures approximately 38 kpc in size (which corresponds to  $\sim 7.5$  arcmin at the distance of 17.1 Mpc) and contains

$2.1 \times 10^8 M_\odot$ . Furthermore, van Driel et al. (1988) determine the HI mass of NGC4026  $\leq 0.71 \times 10^8 M_\odot$ , UGC06956 =  $5.1 \times 10^8 M_\odot$ , UGC06922 =  $4.9 \times 10^8 M_\odot$  and UGC06917 =  $1.28 \times 10^9 M_\odot$ . We detect NGC4026, UGC06956 and the HI filament combined in HIJASS J1158+50 and we measure an HI mass of  $7.94 \times 10^8 M_\odot$  – this matches the total HI mass measured by van Driel et al. (1988) within 1 per cent. Regarding UGC06922 and UGC06917, we measure an HI mass of  $6.17 \times 10^8 M_\odot$  and  $1.58 \times 10^9 M_\odot$ , respectively. One may expect to measure a larger HI flux using a single dish telescope compared to van Driel et al. (1988) using WSRT. However, the HI content of UGC06922 is likely confused as UGC06956 lies in close vicinity.

High resolution observations of this system conducted with the VLA D-array (Verheijen & Zwaan 2001) reveal an HI filament of  $\sim 97$  kpc in size (which corresponds to  $\sim 18$  arcmin and indicated by a cross in Figure 12). The origin of the HI filament is likely to be tidally stripped gas of NGC4026. Verheijen & Zwaan (2001) note that all three bright lenticular galaxies in the Ursa Major cluster including NGC4026 have disturbed HI.

Another intriguing HI extension in the Ursa Major cluster is seen in the NGC4111 system, which has already been studied by Verheijen & Zwaan (2001; VLA D-array). There are six previously catalogued galaxies as listed in NED within 20 arcmin angular separation and within  $150 \text{ km s}^{-1}$  of the central HI velocity (see Figure 12). NGC4111 is also one of the three brightest lenticular galaxies in the Ursa Major cluster with disturbed HI (Verheijen & Zwaan 2001). The HI extends approximately 122 kpc (which corresponds to  $\sim 28$  arcmin at the distance of 15.0 Mpc; Tully et al. 2009 and indicated by a cross in Figure 12) south of the projected central position of NGC4111 (Verheijen & Zwaan 2001). Furthermore, the disturbed HI connects NGC4111 with its close neighbouring galaxies NGC4117 and NGC4118.

The third of the brightest lenticular galaxy in the Ursa Major cluster with disturbed HI content according to Verheijen & Zwaan

(2001) – NGC3998 – lies just outside the HIJASS data cubes at Dec.  $\delta \approx 55^{\circ}27'13''$ .

We do not find any H I detections with extended H I envelopes outside the Ursa Major cluster as defined by Tully et al. (1996).

#### 4.5 Comparison to large area blind HI surveys

Blind H I surveys have the potential for detecting previously uncatalogued galaxies and H I clouds. The two largest blind H I surveys to date are HIPASS (Staveley-Smith et al. 1996, Barnes et al. 2001, Koribalski et al. 2004, Meyer et al. 2004) and ALFALFA (Giovanelli et al. 2005, Haynes et al. 2011). While the HIPASS catalogues contain numerous sources without optical or infrared counterpart (e.g. in regions of high Galactic extinction), there is no evidence for any optically dark galaxies (Ryan-Weber et al. 2002, Koribalski et al. 2004). One of the most massive star-less H I clouds is HIPASS J0731-69 ( $M_{\text{HI}} \sim 10^9 M_{\odot}$ ; Ryder et al. 2001). It is located near the asymmetric spiral galaxy NGC 2442 in the NGC 2434 group. A possible scenario for its origin is discussed in Bekki et al. (2005). Australia Telescope Compact Array (ATCA) observations by Ryder & Koribalski (2004) reveal several H I clumps that are probably embedded in a common envelope of diffuse H I. A group of H I clouds found around 400 km s<sup>-1</sup>, including HIPASS J1712-64 (Kilborn et al. 2000), HIPASS J1718-59 and HIPASS J1616-55 (Koribalski et al. 2004), are likely tidal debris related to the Magellanic Clouds and the Leading Arm. In areas of high stellar density and dust obscuration, it can be difficult to detect optical or infrared counterparts to H I-detected galaxies. Apart from the Galactic Plane, other sources — like the Magellanic Clouds — may hide the stellar component of galaxies. An example is HIPASS J0546-68 ( $v_{\text{sys}} = 1306 \text{ km s}^{-1}$ ) behind the LMC (Ryan-Weber et al. 2002).

The ALFALFA 40 per cent survey has detected nearly 16,000 H I sources in the velocity range from -470 to  $\sim 18,000 \text{ km s}^{-1}$  (Haynes et al. 2011), among these are 1013 sources without assigned optical counterparts. Of the latter, 814 are at velocities from -470 to  $\sim 340 \text{ km s}^{-1}$ , i.e. likely to be HVCs. The remaining are H I cloud candidates, with  $\sim 75$  per cent located near galaxies of similar redshifts (e.g. Leo Ring, Stierwalt et al. 2009). About 50 candidates (0.3 per cent) for isolated H I clouds remain; these require follow-up optical and interferometric H I observations to identify their nature.

In our survey of the Ursa Major region we were able to confirm just one H I source without a definite optical counterpart (HIJASS J1219+46;  $v_{\text{sys}} \sim 392 \text{ km s}^{-1}$ ). It is located near the peculiar galaxy NGC 4288 (HIJASS J1220+46;  $v_{\text{sys}} \sim 520 \text{ km s}^{-1}$ ; also see Wilcots et al. 1996 and Kovač et al. 2009) in the Canes Venatici region. This H I source is discussed in more detail in Section 3.4. The nature of this H I source could be a dwarf companion or tidally stripped gas. H I imaging and deep optical follow-up will be required to determine the true nature.

## 5 SUMMARY

The first blind H I survey of the Ursa Major region was conducted in 2001–2002 as part of HIJASS. The nearby Ursa Major region is within a velocity range from 300 to 1900 km s<sup>-1</sup> and covers an area of  $\sim 480 \text{ deg}^2$ . Using the automated source finder DUCHAMP we identify 166 H I sources in the data based on their peak flux density. The measured H I properties of the sources are presented

in a comprehensive catalogue. We address the catalogue completeness and reliability – we find that the catalogue is 95 per cent complete above our peak flux density cut (33 mJy). The H I mass limit of the catalogue is  $2.5 \times 10^8 M_{\odot}$  (assuming a velocity width of 100 km s<sup>-1</sup> and a distance of 17.1 Mpc).

The catalogue includes 165 H I sources for which optical counterparts are identified using NED and SDSS. We find multiple counterparts within the gridded beam for 33 per cent of the H I detections, which are candidates for galaxy-galaxy interactions. There are 21 high-probability interacting systems – about half of these are within the Ursa Major cluster and have been studied by Verheijen & Sancisi (2001). It is remarkable that the Ursa Major cluster as defined by Tully et al. (1996) only comprises approximately 12 per cent of the surveyed volume discussed in this paper but contains about half of all high-probability candidates for galaxy-galaxy interactions. We discuss four examples of interacting systems, two of which show intriguing extended H I content. The latter have been already been studied with higher resolution and revealed H I filaments and H I distortions of the bright lenticular galaxies.

The HIJASS data contain 10 H I sources that are newly detected in the 21-cm emission line. One of these does not have a visible associate optical counterpart and is likely to be a candidate galaxy/H I cloud. This previously uncatalogued H I source requires follow-up observations to investigate its nature.

## ACKNOWLEDGMENTS

We thank the HIJASS team for providing the data. HIJASS was funded by the UK PPARC (Grant No. PPA/G/S/1998/00620 to Cardiff). We also acknowledge the UK PPARC (Grant No. GR/K28237 to Jodrell Bank) that funded the multibeam receiving system at Jodrell Bank. We thank David Barnes and Mark Calabretta for their help with the fake source injection into the raw data. We thank Felix James ‘Jay’ Lockman for his help with the Green Bank Telescope follow-up observations from setting up, execution to the data reduction. We thank Emma Ryan-Weber, Glenn Kacprzak and the anonymous referee for useful comments. This research has made use of the NASA/IPAC Extragalactic Database, which is operated by the Jet Propulsion Laboratory, California Institute of Technology, under contract with the National Aeronautics and Space Administration. Digitized Sky Survey material is acknowledged, which was produced at the Space Telescope Science Institute under US Government grant NAG W-2166. This research has also made use of the Sloan Digital Sky Survey (SDSS). Funding for the SDSS and SDSS-II was provided by the Alfred P. Sloan Foundation, the Participating Institutions, the National Science Foundation, the U.S. Department of Energy, the National Aeronautics and Space Administration, the Japanese Monbukagakusho, the Max Planck Society, and the Higher Education Funding Council for England. The SDSS was managed by the Astrophysical Research Consortium for the Participating Institutions.

## REFERENCES

- Aihara, H., Allende Prieto, C., An, D., et al. 2011, *ApJS*, 195, 26
- Allsopp, N. J. 1979, *MNRAS*, 188, 765
- Andreon, S., & Ettori, S. 1999, *ApJ*, 516, 647
- Appleton, P. N., & Davies, R. D. 1982, *MNRAS*, 201, 1073

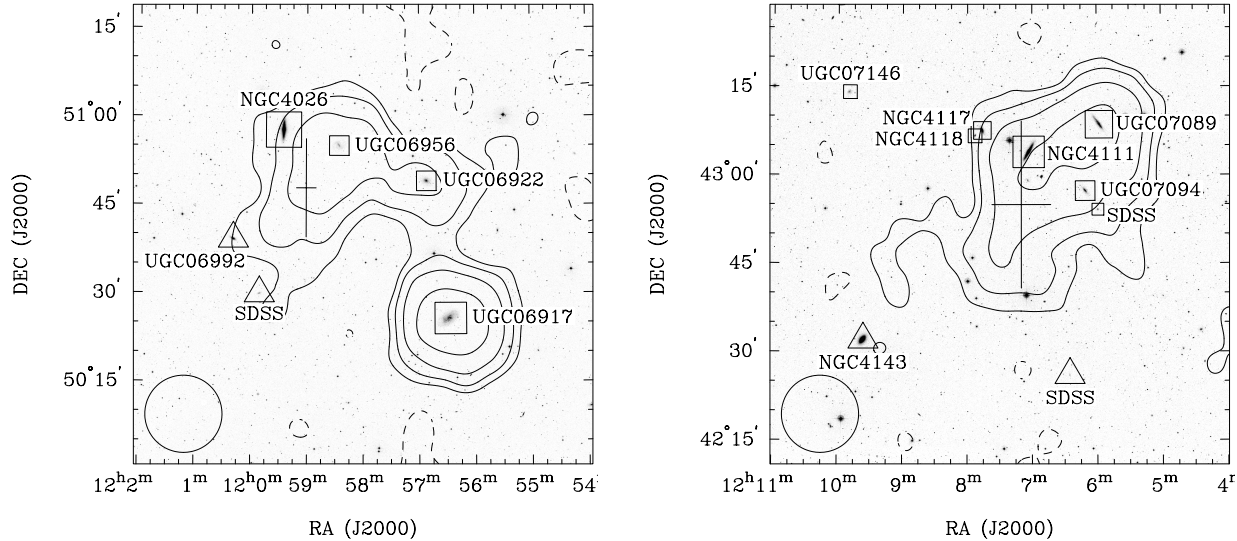


**Figure 12. Two Ursa Major subregions with extended HI content.** We show DSS2 B-band images ( $1.3^\circ \times 1.3^\circ$ ) with overlaid HI intensity contours at  $\pm 1.5, 3, 6$  and  $12 \text{ Jy beam}^{-1} \text{ km s}^{-1}$ . Negative contour levels are indicated with dashed lines. The beam ( $13.1$  arcmin) is indicated in the bottom left corner of each image. (*left:*) The NGC4026 group at approximately  $800 - 1050 \text{ km s}^{-1}$ . The contour lines include 4 catalogued galaxies as indicated by boxes and labelled in the Figure. The galaxies marked with triangles, UGC06992 and SDSSJ115950.83+502955.0, are below the HI sensitivity of this catalogue. The HI filament is indicated by a cross - the extent of the HI filament is similar to the cross size. (*right:*) The NGC4111 group at approximately  $650 - 950 \text{ km s}^{-1}$ . The contour lines include six previously catalogued galaxies as listed in NED (marked with boxes and labelled in the Figure). The disturbed HI content of NGC4111 and its extent is indicated by a cross. We also show two galaxies (at similar velocities than the NGC4111 group) that are not detected in HIJASS (triangles). We note that UGC07146 (in the top left corner) is detected for the first time in the 21-cm emission line (with a systemic velocity of  $1057 \text{ km s}^{-1}$  and therefore outside the displayed velocity range).

Auld, R., Minchin, R. F., Davies, J. I., et al. 2006, MNRAS, 371, 1617  
 Barnes, D. G., et al. 2001, MNRAS, 322, 486  
 Becker, R. H., White, R. L., & Helfand, D. J. 1995, ApJ, 450, 559  
 Bekki, K., Koribalski, B. S., Ryder, S. D., & Couch, W. J. 2005, MNRAS, 357, L21  
 Butcher, H., & Oemler, A., Jr. 1984, ApJ, 285, 426  
 Butcher, H., & Oemler, A., Jr. 1978, ApJ, 219, 18  
 Cappellari, M., Emsellem, E., Krajnović, D., et al. 2011, MNRAS, 416, 1680  
 Chung, A., van Gorkom, J. H., Kenney, J. D. P., Crowl, H., & Vollmer, B. 2009, AJ, 138, 1741  
 Colless, M., Dalton, G., Maddox, S., et al. 2001, MNRAS, 328, 1039  
 De Propriis, R., Colless, M., Peacock, J. A., et al. 2004, MNRAS, 351, 125  
 Disney, M. J. 1976, Nature, 263, 573  
 Dressler, A. 1980, ApJ, 236, 351  
 English, J., Koribalski, B., Bland-Hawthorn, J., Freeman, K. C., & McCain, C. F. 2010, AJ, 139, 102  
 Fairley, B. W., Jones, L. R., Wake, D. A., et al. 2002, MNRAS, 330, 755  
 Fouqué, P., Durand, N., Bottinelli, L., Gougenheim, L., & Paturel, G. 1990, A&AS, 86, 473  
 Gavazzi, G., Boselli, A., van Driel, W., & O’Neil, K. 2005, A&A, 429, 439  
 Giovanelli, R., & Haynes, M. P. 1985, ApJ, 292, 404  
 Giovanelli, R., et al. 2005, AJ, 130, 2598  
 Gómez, P. L., Nichol, R. C., Miller, C. J., et al. 2003, ApJ, 584, 210

Haynes, M. P., Giovanelli, R., Martin, A. M., et al. 2011, AJ, 142, 170  
 Hoffman, G. L., Salpeter, E. E., Farhat, B., et al. 1996, ApJS, 105, 269  
 Kilborn, V. A., Staveley-Smith, L., Marquarding, M., et al. 2000, AJ, 120, 1342  
 Kilborn, V. A., Koribalski, B. S., Forbes, D. A., Barnes, D. G., & Musgrave, R. C. 2005, MNRAS, 356, 77  
 Kilborn, V. A., Forbes, D. A., Koribalski, B. S., Brough, S., & Kern, K. 2006, MNRAS, 371, 739  
 Kilborn, V. A., Forbes, D. A., Barnes, D. G., Koribalski, B. S., Brough, S., & Kern, K. 2009, MNRAS, 400, 1962  
 Koribalski, B. S. 2001, Gas and Galaxy Evolution, 240, 439  
 Koribalski, B. S., & López-Sánchez, Á. R. 2009, MNRAS, 400, 1749  
 Koribalski, B., & Manthey, E. 2005, MNRAS, 358, 202  
 Koribalski, B. S., & Staveley-Smith, L. 2009, ASKAP Science Proposal  
<http://www.atnf.csiro.au/research/WALLABY/proposal.html>  
 Koribalski, B. S., et al. 2004, AJ, 128, 16  
 Kovač, K., Oosterloo, T. A., & van der Hulst, J. M. 2009, MNRAS, 400, 743  
 Lang, R. H., et al. 2003, MNRAS, 342, 738  
 Lewis, I., Balogh, M., De Propriis, R., et al. 2002, MNRAS, 334, 673  
 Margoniner, V. E., de Carvalho, R. R., Gal, R. R., & Djorgovski, S. G. 2001, ApJ, 548, L143  
 McIntyre, V., Star formation and internal kinematics of irregular galaxies, PhD thesis, Department of Engineering Physics, University of Wollongong, 2003.  
<http://ro.uow.edu.au/theses/356>

- Mei, S., Blakeslee, J. P., Côté, P., et al. 2007, *ApJ*, 655, 144
- Metevier, A. J., Romer, A. K., & Ulmer, M. P. 2000, *AJ*, 119, 1090
- Meurer, G. R., Hanish, D. J., Ferguson, H. C., et al. 2006, *ApJS*, 165, 307
- Meyer, M. J., et al. 2004, *MNRAS*, 350, 1195
- Minchin, R. F., Disney, M. J., Boyce, P. J., et al. 2003, *MNRAS*, 346, 787
- Morganti, R., de Zeeuw, P. T., Oosterloo, T. A., et al. 2006, *MNRAS*, 371, 157
- Omar, A., & Dwarakanath, K. S. 2005, *Journal of Astrophysics and Astronomy*, 26, 1
- Oosterloo, T., & van Gorkom, J. 2005, *A&A*, 437, L19
- Rosenberg, J. L., & Schneider, S. E. 2000, *ApJS*, 130, 177
- Ryan-Weber, E., Koribalski, B. S., Staveley-Smith, L., et al. 2002, *AJ*, 124, 1954
- Ryder, S. D., & Koribalski, B. S. 2004, *Recycling Intergalactic and Interstellar Matter*, 217, 44
- Ryder, S. D., et al. 2001, *ApJ*, 555, 232
- Sault, R. J., Teuben, P. J., & Wright, M. C. H. 1995, *Astronomical Data Analysis Software and Systems IV*, 77, 433
- Schombert, J. M., Bothun, G. D., Schneider, S. E., & McGaugh, S. S. 1992, *AJ*, 103, 1107
- Simon, J. D., & Geha, M. 2007, *ApJ*, 670, 313
- Solanes, J. M., Manrique, A., García-Gómez, C., et al. 2001, *ApJ*, 548, 97
- Springel, V., White, S. D. M., Jenkins, A., et al. 2005, *Nature*, 435, 629
- Springob, C. M., Haynes, M. P., & Giovanelli, R. 2005, *ApJ*, 621, 215
- Staveley-Smith, L., et al. 1996, *PASA*, 13, 243
- Stierwalt, S., Haynes, M. P., Giovanelli, R., et al. 2009, *AJ*, 138, 338
- Taylor, E. N., & Webster, R. L. 2005, *ApJ*, 634, 1067
- Toribio, M. C., Solanes, J. M., Giovanelli, R., Haynes, M. P., & Martin, A. M. 2011, *ApJ*, 732, 93
- Trentham, N., Tully, R. B., & Verheijen, M. A. W. 2001, *MNRAS*, 325, 385
- Tully, R. B. 1987, *ApJ*, 321, 280
- Tully, R. B., Verheijen, M. A. W., Pierce, M. J., Huang, J.-S., & Wainscoat, R. J. 1996, *AJ*, 112, 2471
- Tully, R. B., Shaya, E. J., Karachentsev, I. D., et al. 2008, *ApJ*, 686, 1523
- Tully, R. B., Rizzi, L., Shaya, E. J., et al. 2009, *AJ*, 138, 323
- van Driel, W., et al. 1988, *A&A*, 199, 41
- Verheijen, M. A. W., & Sancisi, R. 2001, *A&A*, 370, 765
- Verheijen, M. A. W., & Zwaan, M. 2001, *Gas and Galaxy Evolution*, 240, 867
- Westmeier, T., Popping, A., & Serra, P. 2011, arXiv:1112.3093
- White, S. D. M., & Rees, M. J. 1978, *MNRAS*, 183, 341
- Whiting, M. 2012, *MNRAS*, in press (arXiv:1201.2710v1)  
<http://www.atnf.csiro.au/people/Matthew.Whiting/Duchamp>
- Wilcots, E. M., Lehman, C., & Miller, B. 1996, *AJ*, 111, 1575
- Wong, O. I., et al. 2006, *MNRAS*, 371, 1855
- Wong, O. I., Webster, R. L., Kilborn, V. A., Waugh, M., & Staveley-Smith, L. 2009, *MNRAS*, 399, 2264
- Yahil, A., Tammann, G. A., & Sandage, A. 1977, *ApJ*, 217, 903
- Zwaan, M. A., Briggs, F. H., Sprayberry, D., & Sorar, E. 1997, *ApJ*, 490, 173
- Zwaan, M. A., Verheijen, M. A. W., & Briggs, F. H. 1999, *PASA*, 16, 100
- Zwaan, M. A., et al. 2004, *MNRAS*, 350, 1210